NORTH CAROLINA
STATE UNIVERSITY
RALEIGH, NORTH CAROLINA

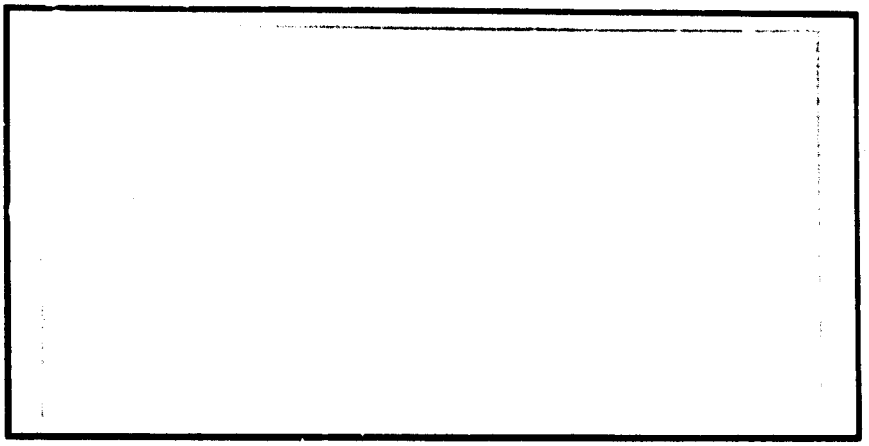

PREPARED FOR
OFFICE OF NAVAL RESEARCH
DEPARTMENT OF THE NAVY
CONTRACT N00014-68-A-0187

Materials Response Phenomena At High Deformation Rates

SPONSORED BY
ADVANCED RESEARCH PROJECTS AGENCY
ARPA ORDER NO. 1090

NORTH CAROLINA STATE UNIVERSITY
Raleigh, North Carolina

FRACTOGRAPHIC AND THERMAL ANALYSES OF SHOCKED ALUMINA

H. Palmour III **D. R. Johnson**
C. H. Kim **C. E. Zimmer**

Technical Report 69-5 **April 1969**

Prepared for

Office of Naval Research
Contract N00014-68-A-0187
NR 064-504

1 September 1967 - 31 August 1971

under a project entitled

MATERIALS RESPONSE PHENOMENA AT HIGH DEFORMATION RATES

sponsored by

Advanced Research Projects Agency
ARPA Order No. 1090

ABSTRACT

This report is concerned with energy absorption processes in ceramic materials exposed to highly dynamic strains capable of causing fracture. Optical and electron fractographic analyses, and direct transmission electron microscopy, were employed in characterizing fracture in ballistically damaged sapphire single crystals and alumina ceramics. Impact fractures were compared with slow break fractures in bars cut from large polycrystalline fragments. Using electron microscopic and dynamic differential calorimetry techniques, explosively shocked alumina particulate also have been examined for evidences of residual strain and annealable excess energy.

The findings produced many mutually supporting evidences of local plastic deformation and energy absorption associated with fracture processes in aluminum oxide ceramics and sapphire single crystals. It was concluded that truly brittle cracks - those which can be propagated with fracture surface energy (γ_f) comparable to the calculated surface free energy (γ_s) without doing work upon the bulk of the material traversed - are relatively rare in this refractory oxide. Rather, fractures commonly observed in α-Al_2O_3 were propagated (at least in part) as almost ductile or blunted cracks - those in which the fracture surface energy (γ_f) has been substantially increased above the nominal surface free energy (γ_s) because of plastic work energy (γ_p) which has to be expended in deforming bulk material at and near the advancing crack front. Microscopic evidences from replication fractography, and particularly from direct transmission electron microscopy, strongly support the concept of localized plastic deformation processes associated with fracture. Dislocation concentrations ($\sim 10^9$ - $10^{11}/cm^2$) observed in local regions of these fracture fragments were several orders of magnitude higher than those normally encountered in unworked ceramic materials ($\sim 10^6/cm$) and approach densities ($\sim 10^{12}/cm^2$) which are typical of extensively worked metals. Exothermic energy releases observed during heating of explosively shocked materials over the range 800 - 1200°C were estimated as $\geq$ 14.6 cal/g.

TABLE OF CONTENTS

LIST OF TABLES

LIST OF FIGURES

Page

INTRODUCTION

This physical ceramics study constitutes one part of an overall, interdisciplinary investigation (at both theoretical and experimental levels) of materials response phenomena at high deformation rates. Other phases of the overall effort have been primarily concerned with real time characterizations of events which occur during highly dynamic straining in metals and polymers, i.e., in materials which generally retain their structural integrity while undergoing relatively large permanent deformations. Specific objectives and current findings from other phases of the broad study have reported elsewhere.[1, 2, 3]

Oxide ceramics (and the broad family of minerals and rocks they typify) in general do not retain structural integrity under large plastic strains ($\varepsilon > 0.01$), and are even less likely to do so under impact conditions. They are nominally brittle unless heated to quite high temperatures (typically > 1000°C), and they almost invariably respond to sufficient stresses at all lower temperatures by fracturing. At high deformation rates and with sufficient stress, fracturing in ceramic-like materials is likely to be both complex and intense, amounting in severe cases to quite generalized fragmentation which is almost explosive in character. Traditionally, high deformation rates have been employed in winning rocks and minerals (including the starting materials from which ceramics are made) from the earth by blasting, and in further processing them into finely divided particulates by crushing, grinding, and milling processes which transfer energy primarily by impact and shock.

Yet such nominally brittle ceramic materials in recent years have become widely used in important military applications (e.g., as key ingredients in composite, light-weight armor) because of their surprisingly effective response to high energy, high velocity impact. Even though the ceramic component does fail at and near the point of impact in its own nominally brittle way, such composites have proven capable of dissipating much, if not all, of the hazardous kinetic energy of an impacting projectile.

Clearly, these nominally brittle materials have an elusive, yet significant, quality of impact resistance (specifically, an ability to absorb impact energy), which is somehow associated with their fracture behavior. Because of major descrepancies between measured fracture surface energies and calculated chemical surface energies, it is difficult to understand how a nominally brittle material displaying these significant levels of resistance to impact can be totally brittle in the classical sense of the Griffith crack theory,[4] which equates the release of elastic strain energy only with the chemical surface energy, γ_s, of the new crack surfaces being generated. Because these experimental descrepancies seem too well documented[5, 6, 7, 8] to be lightly dismissed - even in the case of nominally brittle ceramics - one is forced to consider, and investigate experimentally, the possibility of additional energy absorption akin to Orowan's[9] plastic work term, γ_p, in the intense stress fields which exist under conditions of quasi-hydrostatic restraint at and near the tips of propagating cracks during impact events.

Consideration of all the possible processes of energy dissipation during such a ballistic impact event in a ceramic material is beyond the scope of this report. It is obvious, however, that several factors stemming from the fracture behavior of the ceramic component itself will be pertinent, or even dominant, to any full description of energy dissipation in such an impacting system. The questions to be answered include:

1. What are the fracture sequences?
2. How long does the fragmenting ceramic material retain sufficient integrity to offer an effective resistance to the impacting object?
3. How much energy can be absorbed by the creation of new fracture surface?
4. Is any of the fracture surface energy associated with local deformation processes capable of redirecting and blunting propagating cracks, and/or of direct storage of energy within the material in the form of defect structures resulting from plastic work?
5. How do these factors relate to the compositions, microstructures, and properties of specific ceramic materials?

Answers to questions 1 and 2 and, in part, to question 3, can only come from experimental data obtained during highly dynamic impact events. A considerable body of evidence of this sort for specific cases pertinent to light weight armor has already been obtained by other investigators[10, 11, 12] through use of various forms of high speed optical and/or flash X-ray photography. The emerging real-time

characterizations of the sequences of macroscopic events occurring during such impacts has provided an important background for this report, serving as a reference framework for systematic correlations of the microstructural features of fracture. [Detailed strain measurements during impact of selected ceramic projectile-target pairs (together with documentations of dynamic fracture behavior and subsequent recovery and analysis of fragments) have been planned for the current year's experimental program. These studies are based upon adaptations of firing apparatus and optical diffraction grating techniques which have been developed at this University and have already demonstrated effectiveness for plastic and metal materials in other phases of this overall study.[1-3]]

For the period covered by this report, the ceramic research effort has been directed primarily at questions 3, 4, and 5. These research concerns are of considerable significance, yet they remain fairly amenable to comparative evaluations of damaged and undamaged material. Furthermore, it has been possible to work primarily with damaged (and undamaged) single crystal and polycrystalline alumina ceramic materials obtained from other investigators studying different aspects of ballistic impact and/or explosively generated shock wave phenomena in ceramics.

In this report, (1) optical and electron optical fractography studies of sheared, spalled, and cracked surfaces produced by ballistic impact events, (2) direct examinations of dislocations and other structural defects in impact produced fragments and explosively shocked particulates by transmission electron microscopy, and (3) thermoanalytical measurements of thermally activated releases of shock-induced internal strain energy have been combined to present convincing evidences of significant levels

of localized crystalline plasticity occurring in alumina ceramic materials under impact conditions at ambient temperature. The pertinence of these findings to the overall objectives of this study, and to other areas of scientific and technological interest (e.g., fracture surface energy investigations, and densification kinetics of ceramic particulates having excess internal energy), is briefly discussed.

REVIEW OF THE LITERATURE

Processing, Structure, and Properties of Ceramics

Recent years have witnessed quite remarkable technological developments in the processing of dense, essential pure, refractory ceramic materials and composites which display high hardness and strength. In general, pure oxide ceramics have high elastic moduli, and develop surprising levels of tensile and/or bending strength. Typical "best values" for polycrystalline aluminum oxide (the best known of these "new ceramics") include $\rho \approx 3.97$g/cc, hardness (K_{100}) ≈ 1600, $E \approx 55 \times 10^6$ psi, $\sigma_c > 500 \times 10^3$ psi, and $\sigma_t \approx 100 \times 10^3$ psi (in bending).[13] Single crystal Al_2O_3, when properly treated to remove surface flaws, has been deformed in bending to 2% elastic strain without fracture,[14] and sapphire whiskers (very small filamentary single crystals) have tensile fracture strengths exceeding 1×10^6 psi.[15] Other ceramics with high strength-weight ratios include magnesium aluminate spinel ($\rho \approx 3.6$g/cc, $E \approx 35 \times 10^6$ psi, $\sigma_c \approx 400 \times 10^3$ psi),[16] boron carbide ($\rho = 2.51$g/cc, $\sigma_c \approx 400 \times 10^3$ psi),[17] and silicon carbide ($\rho = 3.2$g/cc, $\sigma_c \approx 200 \times 10^3$ psi).[17]

When considered on a compressive strength-to-weight ratio, these modern ceramic materials are potentially superior to metals and most other materials. Although most of the pertinent technical information is classified,[18] it is public knowledge that such ceramic substances are now supplanting older, heavier, less effective materials for military applications in composite, lightweight body, aircraft, and vehicle armor.

The past fifteen years have seen much progress in relating high temperature deformation in oxide single crystals, and in a few instances, in polycrystalline ceramics, to the presence and mobility of dislocations

[i.e., comparable to the line defects involved in plastic deformation processes in ductile metals].[19-28] However, until very recently, the predominant evidence favored considering polycrystalline ceramics and all except a few single crystals (e.g., MgO) as being truly brittle at temperatures below red heat.

Plastic creep deformation involving mobile (0001) $[11\bar{2}0]$ dislocations in sapphire (single crystal α-Al_2O_3) at 900°C and higher was first reported in 1954,[19] and subsequently, much additional knowledge has been developed about operative deformation modes and kinetics of deformation.[29-34] Earlier work by Bridgman[35] had demonstrated plastic deformation (or deformation twinning) in sapphire at room temperature under conditions of high pressure hydrostatic constraint. Fracture-free room temperature Knoop indentations aligned with the easy slip direction in sapphire, (0001) $[11\bar{2}0]$ were observed by Palmour, et al.,[36-38] and were related to plastic flow under conditions of compressive hydrostatic restraint. Very recently, very high densities of dislocations (including tangles) have been observed by direct transmission electron microscopy in regions adjacent to and beneath microindentations in sapphire.[39]

All these findings, pointing to the likelihood of energy absorption in plastic processes, even at ambient temperatures under constrained conditions, prompted some investigators[40, 41, 42] to suggest that alumina and related ceramics could no longer be considered as classic brittle materials having fracture behavior which could be described in terms of the Griffith criterion[4]

$$\sigma_f = \sqrt{\frac{2E\,\gamma_s}{\pi c}} \qquad (1)$$

Carniglia[43] has re-examined the alumina bend strength data of Mitchell, Spriggs, and Vasilos[44] in terms of the Petch[45] relationship

$$\sigma_f = \sigma_y + k_y d^{-1/2} \tag{2}$$

where

σ_f = fracture strength

σ_y = yield strength

k_y = proportionality constant associated with yielding phenomena

d = average grain size

finding that (a) the observed strength consistently exceeded the fracture strength calculated for classical Griffith flaws of length comparable to the grain size and (b) that the Petch relationship [i.e., having a finite value for σ_y] was obeyed at all but the largest grain sizes. Carniglia concluded that grain boundary shear was particularly effective in blunting cracks [i.e., increasing ρ, the tip radius]. The profound effect of blunting on fracture strength was expressed in a modified version[43] of the Griffith-Orowan criterion

$$\sigma_f = \left[\frac{2E}{\pi c(1-\nu)} \cdot \frac{g\rho}{a} \cdot (\gamma_s + \gamma_p) \right]^{1/2} \tag{3}$$

where

σ_f = tensile fracture strength

E = Young's modulus of elasticity

ν = Poisson's ratio

c = length of propagatable crack ($\approx d$)

g = geometry factor

ρ = radius of crack tip

a = average interatomic spacing

γ_s = chemical surface energy per unit area

γ_p = plastic energy absorbed per unit area

Another convincing argument for the engineering significance of microstrain processes in ceramics at room temperature comes from the recent work of C. D. Pears.[46] Working with dense polycrystalline alumina in tension at room temperature, and utilizing gas bearings to reduce parasitic stresses to < 1%, he has observed precision elastic limits at only 0.5 σ_f, i.e., at higher stresses, microstrain caused departures from strictly linear elasticity.

Dry ball milled alumina (when contrasted to wet ball milled material)[47] and explosively shocked alumina powders (when contrasted to unshocked)[48] are much more sinterable than the control specimens. In each case, enhancement of sinterability has been empirically correlated with residual strain energy measurable in terms of X-ray line broadening)[47, 49] resulting from the impact process, and one may conclude that excess free energy released during annealing is able to assist in driving the sintering mechanism.[50-52]

Attempts to measure fracture surface energies in alumina have consistently yielded values which greatly exceed the calculated free surface energy, γ_s, normally considered to be about 10^3 ergs/cm^2. The minimum and average surface free energies for α-Al_2O_3 at room temperature were estimated as 1057 ergs/cm^2 and 1136 ergs/cm^2, respectively, from thermodynamic data by Bruce.[53] Congleton and Petch[54] observed temperature-dependent fracture surface energy values in the 25,000 - 30,000 erg/cm^2 range for the $(11\bar{2}3)$ plane of sapphire. They attributed much of the discrepancy between chemical and fracture surface energies

to plastic deformation in the locally intense stress fields near the tip of an advancing crack. Similarly, Wiederhorn[55] has observed abnormally high γ_f values (~ 40,000 ergs/cm^2) in double-cantilever crack propagation studies for the (0001) plane in sapphire (cracks were diverted, since (0001) is not a true cleavage plane). Cleavage was observed on the $(10\bar{1}0)$ prism plane and the $(10\bar{1}2)$ rhombohedral plane with measured fracture surface energy values of 7,300 and 6000 ergs/cm^2, respectively, or about six times larger than Bruce's calculated surface free energies.[53]

Other oxide ceramic systems, particularly those having the spinel structure, are also considered to be likely candidates for significant energy absorption by microstrain processes. Not only does it have an unusually high surface free energy (~ 2208 ergs/cm^2 @ 20°C),[53] but at high temperatures, magnesium aluminate spinel has demonstrated extensive polycrystalline plasticity as a consequence of multiple (111) [110] slip systems,[56, 57] similar to those of f.c.c. metals. Ambient temperature deformation resulting from locally intense stress concentrations (under some constraint within the bulk section) may well have accounted for certain microstructural features characteristic of intersecting slip systems which were observed on polycrystalline spinel fracture surfaces by Palmour, _et al_. (e.g., Figures 28 and 29 of Ref. 58). [Plans for the current contract year include broadening the scope of this study of high deformation rate effects to include spinel ceramics. Spinel materials have been the subject of continuing study in this laboratory.[59-62]]

Fractography*

To understand fracture, one must be able to measure and predict all the forces and properties in the entire system, whether they be such large-scale factors as the gross dynamics of an impacting system or the stiffness of testing equipment, intermediate scale factors such as stress concentration(s) at the root of a notch, or fine-scale factors such as the resolved shear forces necessary to move individual dislocations. Research work with simple materials such as ionic crystals and metallic single crystals has resulted in some understanding of the basic mechanisms of fracture. On another scale, numerous mechanical tests of engineering materials have been performed in order to evaluate and select materials for the rational design of useful and reliable structures. Thus, present knowledge progresses from both ends of the currently known spectrum of interest--from understanding of bonding strength between just two atoms to characterizations of plane-strain fracture toughness in massive specimens. Though progress is being made in both the physics of materials and the continum mechanics approaches, researchers in the two fields have not been able fully to benefit from one another's findings. This is partly due to the microstructural complexities of the practical structural materials typically investigated in fracture mechanics studies, and partly attributable to great differences in scale (macro- versus micro-) between some of the factors of concern in these two approaches.

---

*In addition to papers specifically mentioned in this section, the List of References includes several very helpful general references on electron fractography.[113-116]

Visual and low-magnification observations of fracture surfaces have been utilized for many years to assist engineers in fracture analysis. Powerful new means of fracture investigation have come to prominence within the past decade as a consequence of the growing use of high resolution electron microscopy.

By examining fracture surfaces at high magnification with the electron microscope, one can determine the relationships between surface topography and microstructure, as well as the chronological order of fine-scale events taking place during fracture. Electron microscopy helps in bridging the gap between physical metallurgy (or physical ceramics) and continum mechanics by providing qualitative assessments of fracture processes occurring at the micron (and even sub-micron) scale, and by yielding quantitative measurements of some of the fracture variables that are not readily measured in either of the aforementioned macro- or micro-scale approaches.

When fracture surfaces are observed at increasingly higher magnifications, the extremely complex nature of the fracture features becomes more and more apparent. Electron fractographs show clearly that structural materials generally cannot be considered as homogeneous continua, and that no simple dislocation models can, by themselves, entirely explain the fracture processes. However, in spite of the complex appearance of a fracture surface, it is possible to see at high magnification that a given mechanism of fracture is associated with a certain number of characteristic fracture features, as cited by Zapffe.[63]

Nomenclature*

Certainly, combinations of various materials and various fracture conditions are bound to result in a very wide range of different fracture-surface features. These many different features, when being viewed at higher and higher magnifications, can be differentiated again and again, and classified into a whole array of groups, subgroups, etc. Burghard and Davidson[64] examined the factors involved in a fine-scale fracture process and concluded that specification of three characteristics are necessary for the complete description of the fracture; i.e., the basic mechanism involved, the relationship of the fracture path to the microstructure, and the macroscopic features of the fracture. They suggested the following classification:

(1) Basic Mechanism

   a. plastic fracture

   b. cleavage

   c. fatigue

(2) Fracture Mode

   a. transgranular

   b. intergranular

---

*One of the basic premises of this study is that crystalline ceramics like alumina are not totally brittle in their fracture behavior. It therefore follows that differences in the principal features of fracture topography between such ceramics and the ductile metals are likely to reside only in degree, rather than in kind. For this reason, the nomenclature customarily used in describing metal fracture has been selected for use in this report.

(3) Macroscopic Characteristics

a. ductile

b. brittle

The single feature common to every fracture is the creation of new surface. In the most fundamental sense, such new surface may be created in only two ways; by extensive crystallographic slip or by direct separation normal to specific crystallographic planes. The generic names given the numerous phenomena associated with these two mechanisms are plastic fracture and cleavage, respectively. The disruption of material under the influence of cyclic loading (at some level below the single-stroke breaking load) produces a widely recognized class of failure commonly described as fatigue fracture.

The classification of fracture as to mode concerns the relationship of the fracture path to the microstructure of the material. The advancing crack front takes either a transgranular or an intergranular course through any given volume element, and produces markings which are characteristic of the structure and properties of the region traversed.

Plastic Fracture

The most common type of plastic fracture in metals is the initiation, growth, and coalescence of microvoids. In such cases, microvoids are nucleated at preferred sites, grow under the influence of triaxial stresses, and coalesce by localized internal necking. Such a mechanism creates a fracture surface passing through the center of a sheet of voids, resulting in numerous concave depressions in each fracture surface. Characterization

of such depressions, commonly referred to as "dimples," was first described by Crussard, et al.[65]

The influence of plastic strain conditions on the shape of dimples formed by microvoid coalescence has been investigated extensively by Beachem.[66] Deformation processes related to plastic fracture have been studied in detail by Beachem and Meyn.[67]

Four topographic features [(1) glide plane decohesion, (2) serpentine glide, (3) ripples, and (4) stretching] have been classified and correlated with various stages of plastic deformation of a surface.[67] Glide plane decohesion is that mechanism by which slip occurs predominantly on one set of slip planes, causing an observable amount of new surface to be formed. Serpentine glide is glide plane decohesion on several sets of planes simultaneously. This mechanism is thought to be formed by combinations of pencil or wavy slip, and cross slip, and is often found in polycrystalline materials where deformation in a given grain must accommodate the deformation of neighboring grains. Thus, slip is necessary on multiple planes, giving rise to slip steps which form an interwoven or plaited pattern. Further smoothing out of these steps by plastic deformation leads to the formation of ripples. Subsequent plastic flow creates new surface on which the glide steps are so poorly delineated that the surface appears smooth and featureless. The term stretching is used to describe the processes which generate such surface areas.

Cleavage

Brittle fracture of a perfect crystal would be quite likely to produce flat, featureless fracture surfaces coincident with certain low index crystallographic planes. This form of fracture is called cleavage. Real crystals, however, are never perfect, and a cleavage crack, even if initiated as a single plane, actually is broken into a set of parallel cracks by imperfections.

The propagation of a cleavage crack thus occurs by the simultaneous advance of a number of cracks on different parallel planes. These cracks are joined by steps formed either by secondary cleavage or plastic fracture. Cleavage steps are generally observed to run together in the direction of local crack propagation, producing the familiar, characteristic "river patterns."

A comprehensive review of the nature and significance of the surface markings observed in cleavage fracture has been provided by Low.[68] In this review, it is pointed out that the most common origin of cleavage steps is that of screw dislocations intersecting the cleavage plane. The advance of a planar cleavage crack through a screw dislocation results in a shift of the level of the crack on each side of the dislocation. Low also observed that the density of cleavage steps was increased markedly as the crack passed through a twist boundary, while no change in the number of steps was evident when a crack crossed a pure tilt boundary.

The screw dislocations which give rise to additional cleavage steps may be derived from several sources. They may be part of the network of

grown-in dislocations present in any real crystal or they may be associated with low-angle twist boundaries. In addition, screw dislocations may be introduced by plastic deformation, either by prior deformation of the entire crystal (as by primary or reflected shock waves under impact conditions) or by glide occurring ahead of the advancing cleavage crack.

In polycrystalline aggregates the local direction of crack propagation is often observed to vary from grain to grain. Individual cleavage facets may show directions of propagation nearly opposite to the macroscopic direction of crack propagation.

Conchoidal Fracture

Ceramics are likely to display a very characteristic type of fracture which differs from planar cleavage by being both curvilinear and noncrystallographic. This is called conchoidal fracture, and is typically observed in many non-metals, including the seashells from which its name is derived.

Fatigue

Cyclic propagation of a fatigue crack has been found to produce areas exhibiting a fracture surface topography which is characteristically different from that of other types of fracture. Usually some area of a fatigue fracture may be found which exhibits a series of parallel, though perhaps curved, regularly spaced, line-like fractures oriented normal to the direction of local crack propagation. These features, regardless of profile shape, are called striations.

Transmission Electron Microscopy

The ability to image individual dislocations and other structural defects within thin foils by direct transmission electron microscopy has provided the materials scientist with an extremely powerful arsenal of additional analytical methods for evaluating growth, irradiation damage and deformation processes in crystalline material. Some idea of its significance to ongoing research in metals and in ceramics over the past decade can be gained from a review of selected general references.[69-73]

The contrast effects which permit imaging of these line defects result from differences in electron scattering and diffraction effects in the locally strained regions of the crystal structure near the dislocations. Both interpretive theory and experimental practice for imaging of defects have been described in considerable detail in several valuable texts and papers.[74-78]

The technique is dependent upon the availability of very thin foils ($\sim$ 2000Å for metals, perhaps up to $\sim$ 20,000Å for oxide ceramics with low scattering factors). The chemical inertness and high electrical resistivity of typical ceramic oxides like alumina preclude those thinning techniques based upon etching with aqueous solutions and/or electrolytic action which have been found effective with most metals. Many of the early studies of individual dislocations in alumina were carried out with as-grown and/or thermally etched platelets[79] or filamentary whiskers.[80, 81] For sapphire specimens cut from bulk, chemical thinning techniques which employed hot, highly concentrated phosphoric acid or fused salts as the etchant were

developed by Tighe,[82] Barber and Tighe,[83-85] and Wilks.[86] Ion beam thinning methods originally developed in France[87, 88] have been very successfully adapted to polycrystalline ceramics by Tighe and co-workers.[89, 90, 91]

Dynamic Differential Calorimetry

Residual strain energy (existing in the form of dislocations and/or other structural defects) may be considered as non-thermodynamic excess energy, i.e., the excess is only metastable and should not exist under conditions of true thermodynamic equilibrium. Such strains can, in fact, be reduced or removed by thermal treatments in what are generally called annealing processes.

The energy released during annealing can be detected experimentally by various thermoanalytical methods. The basic method is known as differential thermal analysis (DTA), in which sensitive differential thermocouples are employed to measure slight temperature differences between the sample material and an appropriate (and usually inert) reference material while both are being heated (or cooled) at a uniform rate within a uniform (usually massive) thermal environment. Theories, methods and applications of DTA techniques have been summarized by Smothers and Chaing[92] and by David.[93]

Apparatus for dynamic differential calorimetry (DDC) is based upon a rather different specimen holder geometry featuring a less massive thermal environment. It facilitates quantitative estimates of the total energy involved in the causative process (proportional to the integrated area under the peak for a given energy release or absorption). This valuable modification of the DTA method has been described by David[93] and by Campbell.[94]

MATERIALS

Ballistically damaged specimens of (a) sapphire single crystal and (b) polycrystalline aluminum oxide were obtained from other investigators concerned with impact resistance of potential light weight armor materials. The sapphire specimen was initially 3" dia. x 3/8" thick and had been struck by a 0.30 caliber armor piercing projectile at a velocity sufficient to cause extensive damage and projectile penetration.* The commercially produced polycrystalline alumina ceramic (~ 94% α-Al_2O_3) originally measured 6" x 6" x 3/8" and had been struck by a similar projectile at a velocity (~ 70% higher) sufficient to cause generally comparable damage and penetration.† Both specimens had been cemented to, and were supported by, similar fiber-reinforced backing materials for the test shots.

Fractured fragments were reassembled into the original configuration as well as possible. Macroscopic views of these ballistically damaged specimens are shown in Figures 1 and 2.

Though they would have been of considerable interest, fine fragments from the immediate impact areas in these specimens were not available for this study. As a substitute for ballistically produced fine fragments, explosively shocked alumina particulates,‡ were obtained for thermoanalytical and electron microscopic examinations, together with a control specimen of the original unshocked alumina (Linde A).‡

---

*Specimen provided by Captain David M. Martin, Clothing and Organic Materials Laboratory, Natick Laboratories, U. S. Army, Natick, Mass.

†Specimen provided by Captain McDonald Robinson, Ceramics Laboratory, U. S. Army Mechanics and Materials Research Center, Watertown, Mass.

‡Specimen provided by Dr. Oswald R. Bergmann, Eastern Laboratory, Explosives Department, E. I. du Pont de Nemours & Company, Inc., Gibbstown, New Jersey 08027

‡Alumina Powder, Linde A grade, a product of Linde Division, Union Carbide Corp., East Chicago, Indiana. [Specimen provided by Dr. Bergmann‡]

a. Overall view of reassembled fragments, X1.65.

b. Cleavage detail in fragment marked by arrow in Fig. 1a, X8.3.

Figure 1. Ballistically damaged sapphire single crystal.

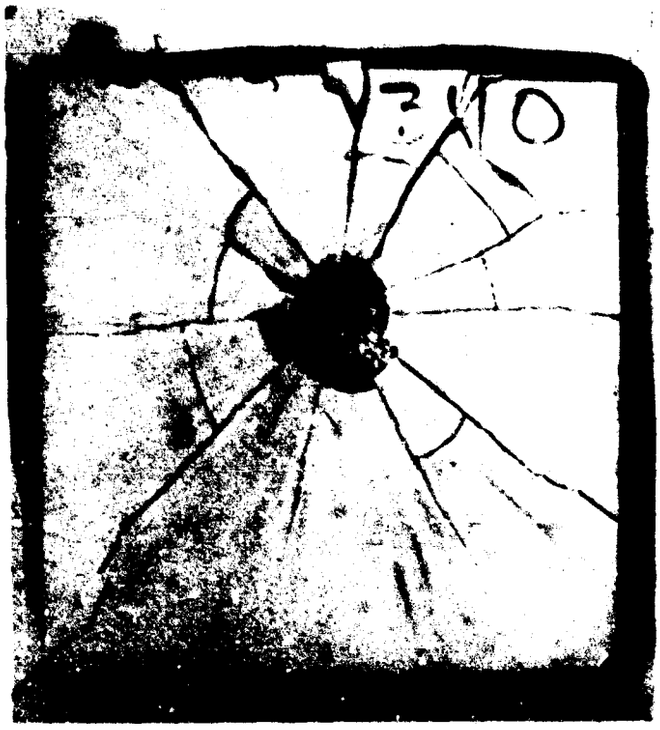

Damage was produced by high velocity impact (.30 cal. AP projectile).

a. Front face of 6" x 6" x 3/8" alumina ceramic tile after impact.

Black adhesive bonded tile to backing material.

Spalled material at back face was retained by adhesive. This portion was removed to reveal late-phase spall cracks shown in Fig. 2.

b. Back face of tile after removal of fiber-reinforced backing.

Figure 2. Ballistically damaged polycrystalline alumina (cont. p. 23).

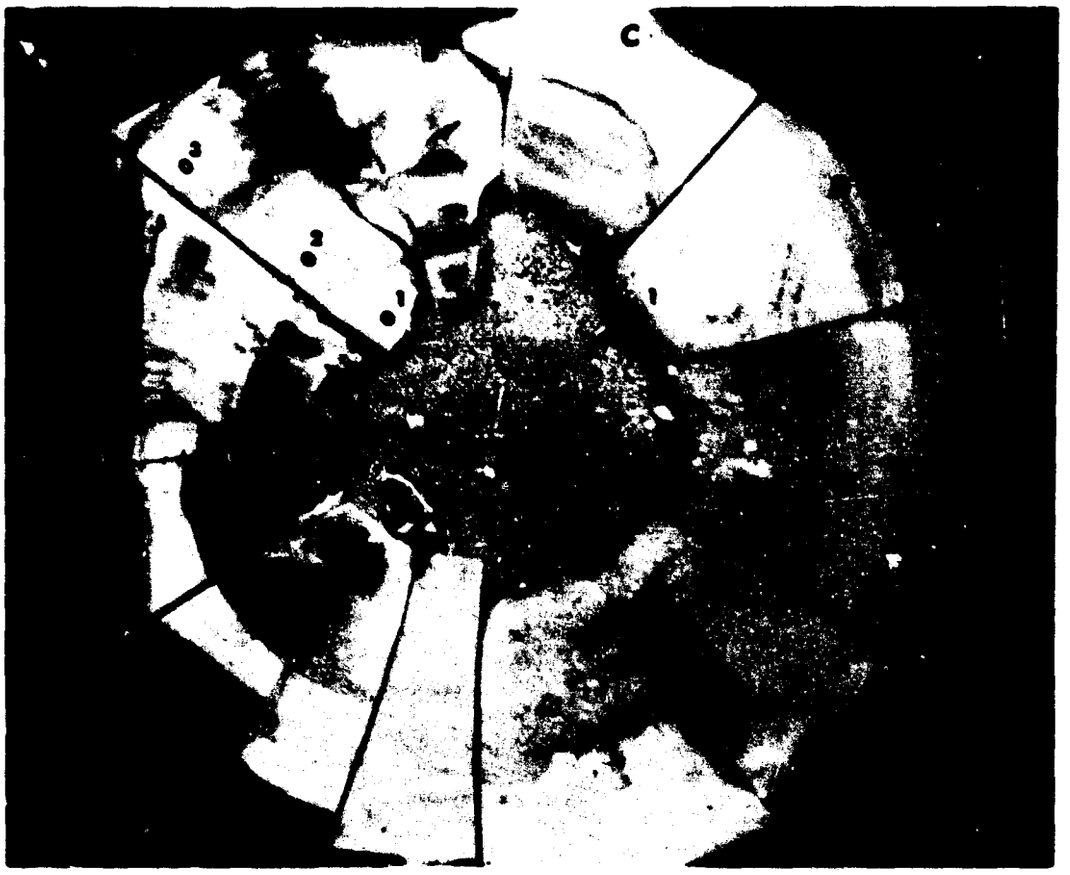

c. Backface of tile after removal of spalled material, X1.6. Numbers identify areas from which surface replicas were taken.

d. Detail of shear conoid surface (arrow) and radial crack for segment D.

Figure 2, cont. Ballistically damaged polycrystalline alumina.

REPLICATION OF FRACTURE SURFACES

The fracture surface being investigated was cleaned with acetone to remove dust or other foreign materials. Surface residues and tiny fracture fragments then were removed by applying, stripping, and discarding plastic replicating tape* two or three times in succession. Thereafter, a small amount of the replication solution† was dropped on the area selected for study and allowed to spread on the surface of the specimen. Replicating tape was applied smoothly over the coated area avoiding bubble entrapment. Light, uniform pressure was applied to the tape during the 3-5 minutes required for evaporation of the solvent.

With tweezers, the replicating tape was carefully stripped off and transferred to a glass microscope slide surfaced with double backed transparent tape. A slide containing many such first replicas was then processed in vacuum coater‡ to produce shadowed carbon second replicas.

The replicas were shadowed with an evaporated thin film of platinum (< 100Å) impinging at 30° for the single crystal replicas and at 45° for polycrystalline replicas.

An evaporated film of amorphous carbon thin enough to be transparent to electrons and strong enough to constitute the second replica was thereafter deposited at an incident angle of 90° without intervening atmospheric exposure.

---

*No. 1134 Replicating Tape, a product of Ernest F. Fullam, Inc., Schenectady, N. Y.

†Replication Solution, a product of Ladd Research Industries, Burlington, Vermont.

‡DV-502 Vacuum Coater, a product of Denton Vacuum, Inc., Cherry Hill, New Jersey.

The shadowed replica film was then cut to fit 1/8" diam specimen support grids, and floated in acetone to dissolve the initial plastic replica. Within 15 to 30 minutes, depending on the thickness of the replicating tape, the plastic was fully dissolved. Completion of this phase was evident when the platinum-shadowed carbon second replica sank to the bottom of the container. The replica was retrieved from the solvent on a copper specimen grid, and allowed to dry by evaporation.

This procedure produced satisfactory replicas of polycrystalline aluminum oxide fracture surfaces. However, with the very angular sapphire fracture surfaces, excessive breaking, particularly at cleavage step edges, of carbon second replicas occurred during dissolution of the plastic first replicas.

To prevent breaking of replicas of sapphire surfaces a protective coating of white petroleum jelly dissolved in carbon tetrachloride solution was applied to the carbon second replica after evaporation, but before dissolution of the first replica, following the method of Brammar and Dewey.[95] An effective thickness of the protective coating was found to be 0.1 - 0.3μm. Coated replica(s) were floated in acetone solution to remove the plastic first replica, and then transferred to grids as described above. Thereafter, the grid-supported second replica was immersed in carbon tetrachloride for five hours to remove the petroleum coating. Replicas cleaned in this way reproduced the single crystal fracture surfaces with fidelity and without undue fragility.

EQUIPMENT

Optical Microscopy

For initial examinations at low magnification (5-160X) a steromicroscope with 35mm photographic capability* was employed. For more detailed studies in the 100-1000X range, a bench microscope† was used. This instrument permits examinations in a variety of incident, transmitted or mixed mode illuminations, and also provides Nomarski phase interference constrast capability of particular value for these studies of surface textures.

Electron Microscopy

The increased depth of focus, high magnification, and high resolving power of the electron microscope are particularly pertinent for these studies since many of the fine details of interest are inaccessible by optical microscopy. All work in this study was done on a high resolution transmission electron microscope with 80, 100, and 120 Kv accelerating voltages, and demonstrable resolution(s) of 4.5Å (small bore pole piece) and 10Å (large bore pole piece).‡ With its full complement of specimen stages and other accessories, this versatile instrument is well suited for fractography and for studies of structural defects by direct transmission in thin foils. [Ion beam thinning capability will be available in the

---

*Reichert MAK-MS Stereoscopic Microscope with LUX-M illuminator, a product of Optische Werke C. Reichert (Vienna), distributed by William J. Hacker & Company, Inc., West Caldwell, N. J.

†Reichert ZETOPAN-M (ZETCIR) Microscope with LUXUS Iodine-Quartz Light Source [also distributed by Hacker, above].

‡JEOLCO JEM-120 Transmission Electron Microscope, a product of Japan Electron Optical Laboratory (Tokyo), distributed by JEOLCO (U. S. A.), Inc., Medford, Mass.

near future to facilitate production of uniform foils of optimum thinness, permitting more exhaustive study of defect structures resulting from high deformation rates in the ceramic materials of interest in this study.]

Dynamic Differential Calorimetry

Dynamic Differential Calorimetry (DDC) was employed to detect and measure the energy stored as annealable defects in explosively shocked alumina. A differential thermal analysis apparatus* was modified for these measurements by the addition of an appropriate sample holder and differential thermocouple.† The ring-type differential thermocouple employed allows the detection of differential signals as small as 0.05 microvolts.

---

*Model DTA-12A Differential Thermal Analysis Apparatus, a product of Robert L. Stone Company [now a Division of Tracor, Inc.], Austin, Texas.

†Type SH-11BB2-PDZ Sample Holder with Pt-Pt 10% Rh ring-type differential thermocouple. Each ring of the thermocouple supports a very small platinum vessel containing specimen or reference, respectively.

RESULTS AND DISCUSSION

Single Crystal α-Al_2O_3

The crystallographic orientation of the sapphire target is presented in Figure 3 in the form of a stereographic projection. This pole figure represents the specimen geometric axis and is coincident with the projectile trajectory responsible for the damage shown in Figures 1a and 1b. It also was approximately parallel with the crystal growth axis. Identities of poles normal to the principal crystallographic planes are designated in Miller-Bravais hexagonal notation, and with reference to the morphological unit cell having a c:a ratio of 1.365:1. These data were determined from Laue' back reflection X-ray photograms, and were indexed by means of PIMAX tables for α-Al_2O_3 developed by Witter and Palmour.[96, 97]

The planar surfaces of the undamaged crystal specimen were nearly parallel with $(20\bar{2}5)$ crystallographic planes. The crystallographic orientation of the specimen impact axis can be represented in terms of (1) an inclination of $\approx 30°$ from the [0001] c-axis toward the $[2\bar{1}\bar{1}0]$ pole, followed by (2) a counterclockwise rotation of $\approx 13°$ from the [0001] - $[2\bar{1}\bar{1}0]$ zone. Alternatively, the axis of impact can be indexed directly at the intercept of two spherical angles, (1) 32.5° from [0001], and (2) 61° from $[2\bar{1}\bar{1}0]$.

Fracture by Rhombohedral Cleavage

The damaged crystal segment first shown in Figure 1b has been indexed by visual inspection in terms of the stereographic projection given in Figure 3. From these examinations, it was found that all the significant crystallographic surface detail could be attributed to cleavage occurring on two first order and two second order rhombohedral planes, $(10\bar{1}1)$, $(\bar{1}011)$ and $(1\bar{1}02)$, $(\bar{1}012)$, respectively. All surfaces not so cleaved appeared to

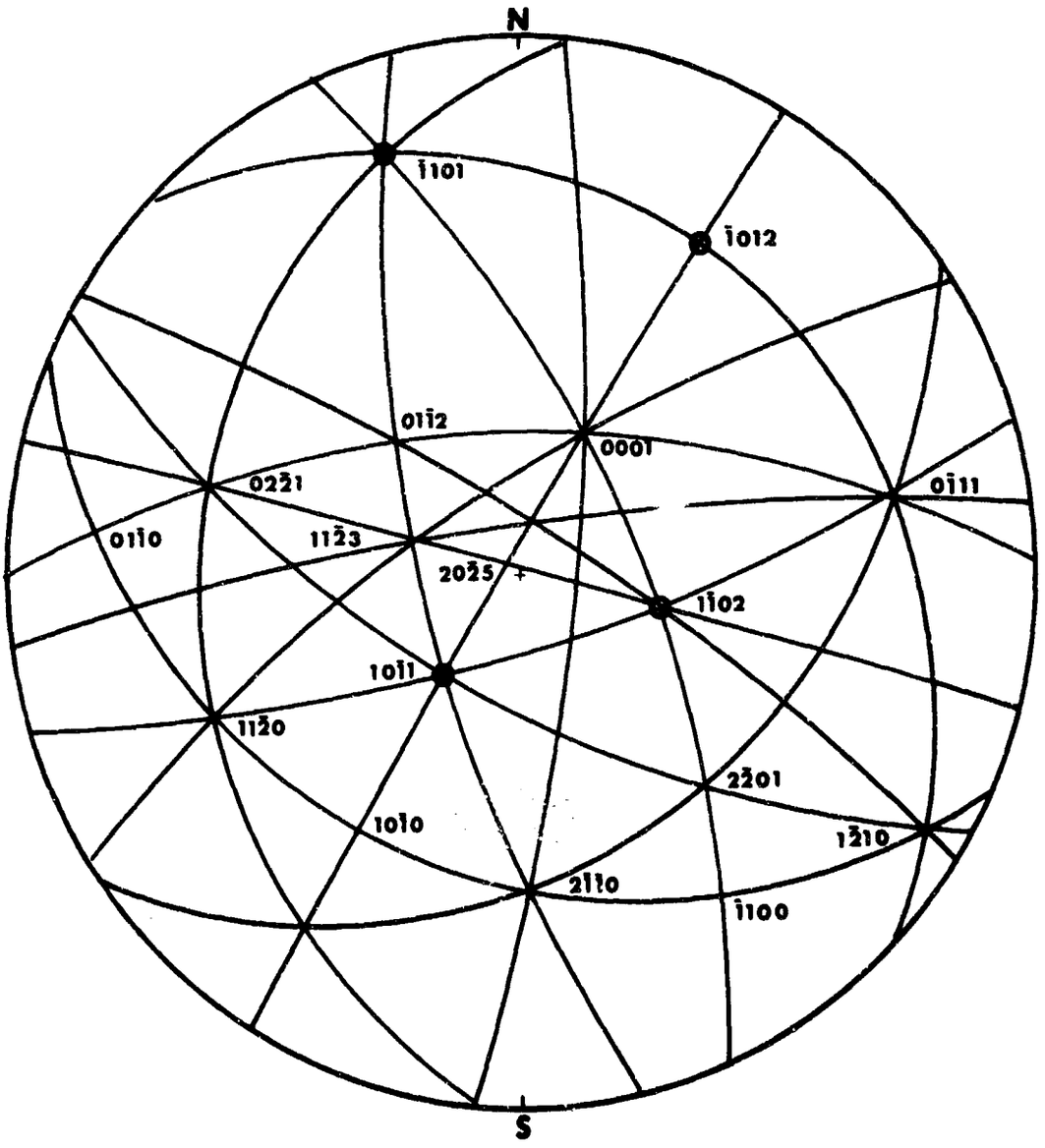

Figure 3. Stereographic projection showing crystallographic orientation for sapphire fragment illustrated in Fig. 1b. Indices are given in Miller-Bravais notation for the morphological unit cell, c/a = 1.365:1. Circled poles correspond to principal cleavage planes (Fig. 4).

have resulted from conchoidal fracture. The first order rhombohedral cleavage surfaces tended to be planar and smooth, while those of second order were finely stepped or striated. Some of the most prominent crystallographic details are identified in Figure 4.

Fracture surfaces lying approximately normal to the impact trajectory show an unique sense of directionality as a consequence of the large number of edge intersections of $(10\bar{1}1)$ and $(1\bar{1}02)$ cleavage planes. These edges are aligned with the $[\bar{1}101]$ direction, and have characteristic included angles of 133°. Included angles existing between the four operative cleavage systems are indicated in Table I. Typical heavily stepped and/or striated fracture textures characteristic of the dominant cleavage modes are illustrated at higher optical magnifications in Figure 5, which indicates excellent correspondence of predicted and observed angular relationships between specific cleavage planes.

Table I. Angular Relationships Between α-Al_2O_3 Cleavage Planes

	Included Angle* Between Indicated Planes			
Planes	$(10\bar{1}1)$	$(1\bar{1}02)$	$(\bar{1}101)$	$(\bar{1}012)$
$(10\bar{1}1)$	--	133.01°	86.02°	84.16°
$(1\bar{1}02)$	133.01°	—	84.16°	115.18°
$(\bar{1}101)$	86.02°	84.16°	--	133.01°
$(\bar{1}012)$	84.16°	115.18°	133.01°	--

Although not evident in Figures 4 and 5, optical examinations of other fragments with finely textured cleavage surfaces in reflected or transmitted illumination showed considerable evidence of interference fringes adjacent to cleavage steps. These fringes are indicative of cracks extending along

*Included angle between planes is $(180°-\theta°)$, where θ is the angle between poles (normals) to the planes as plotted on the stereographic projection. Values for θ taken from Table II, Ref. 97.

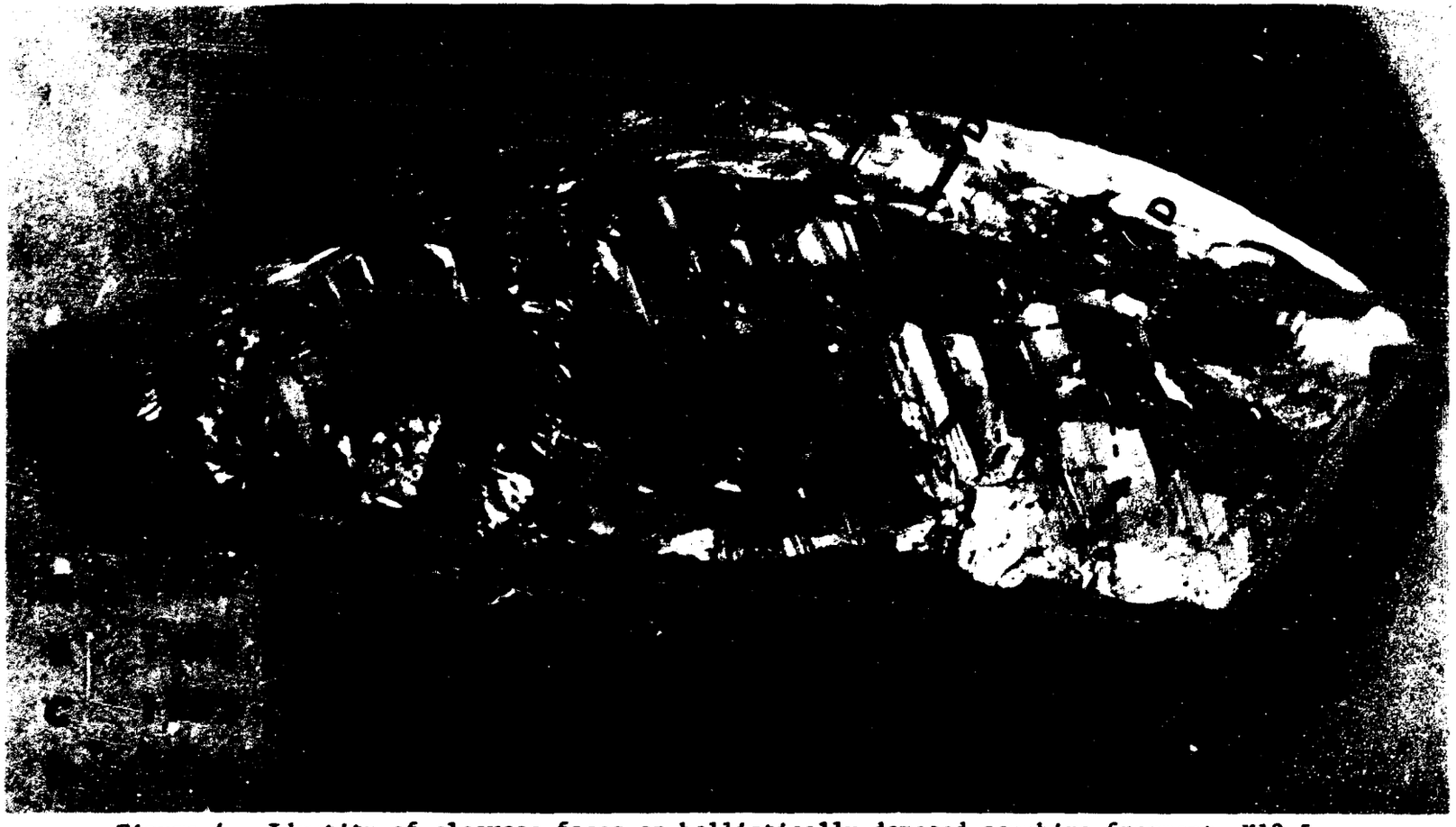

Figure 4. Identity of cleavage faces on ballistically damaged sapphire fragment, X12.5. Arrows superposed on this enlarged view of Fig. 1b indicate traces of the poles circled on the stereographic projection in Fig. 3. Enclosed area at right locates Fib. 5.

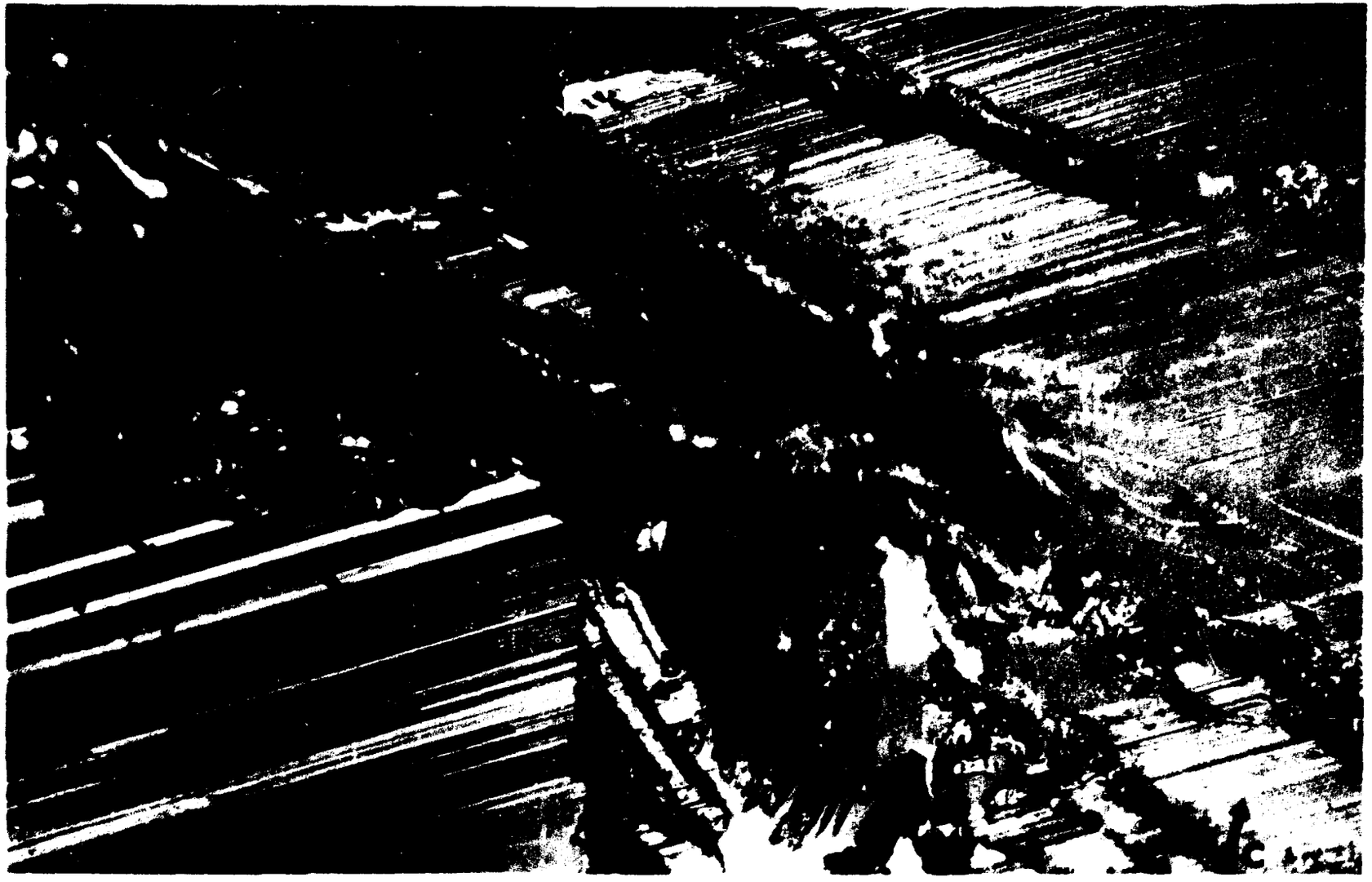

Figure 5. Fracture topography resulting from rhombohedral cleavage in one magnified portion of Fig. 4. Arrows identify A: $(10\bar{1}1)$, B: $(\bar{1}101)$, C: $(\bar{1}102)$ and D: $(\bar{1}012)$ rhombohedral cleavage planes. Reflected light, Nomarski phase interference contrast, ~ X100.

original cleavage surfaces for additional distances beneath the steps. In such cases, it is reasonable to conclude that (1) the break causing an externally visible cleavage step occurred as a consequence of a state of stress which included a bending moment, (2) the crack extending beneath the step along the original cleavage plane was arrested within the bulk after the driving force had been decoupled by the aforementioned break, and (3) the true area of new surface generated by such cleavages must exceed the total externally visible surface. Similar cracks under-running cleavage steps in MgO single crystals have been described by Lewis,[98] who indicated that an overlap of cleavage crack segments appears to occur prior to step formation, and suggested that additional elastic energy absorption would be possible in such processes.

Replication Fractography

The same basic fracture textures stemming from cleavages are maintained, only on finer scales, at the higher magnifications available in electron microscopic examinations of plastic-carbon two stage replicas. In Figure 6, the dominant stepped texture results from three different cleavage planes intersecting at almost orthogonal angles, and is consistent with the expected angular relationships (Table I).*

In some regions, the cleavage steps are less distinct, as in Figure 7, In this case the steps between cleavage surfaces take three forms: they are (a) cleaved at ~ 133° ($\theta \approx 47°$), or (b) parted (a fracture mode which is

---

*Identities of specific planes and directions have not always been retained through all the stages of replicating, transferring, and magnifying involved in electron microscopic fractography. The four sets of rhombohedral planes previously identified certainly dominate the cleavage textures, but other, less favorably oriented rhombohedral planes may have contributed to the fine textures.

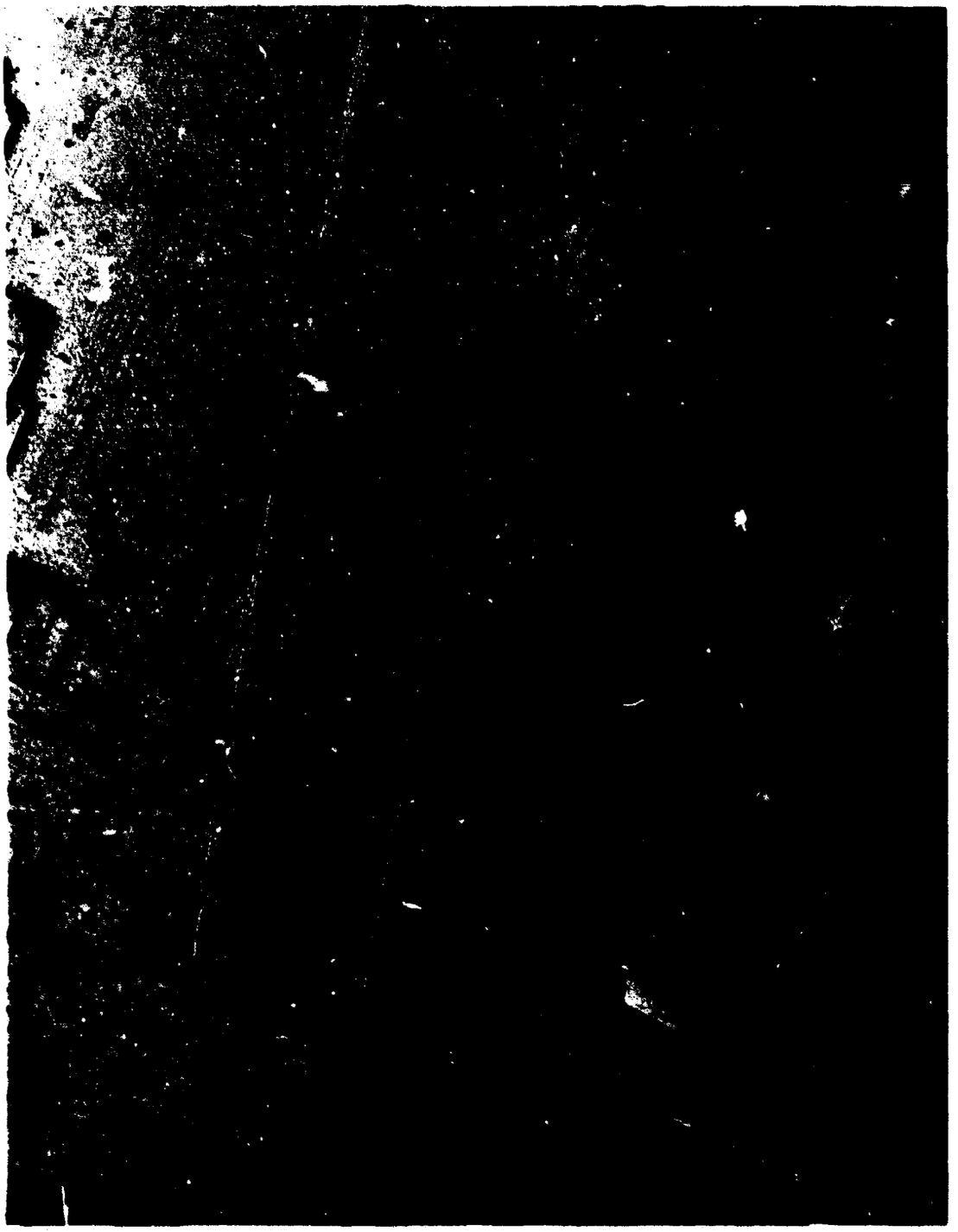

Figure 6. Cleavage fractography in ballistically damaged sapphire, X12,000. Two stage plastic-carbon replica, Pt-shadowed at 45° [S2-582].* The three dimensional, almost orthogonal intersections of sets of rhombohedral planes (two first order and one second order) form the basic stepped texture. Arrow indicates other typical oblique intersections between first and second order rhombohedral planes.

*Bracketed characters identify replica (S2) and electron image plate (582).

Figure 7. Cleavage step variations in ballistically damaged sapphire, X15,000. Two stage plastic-carbon replica, Pt-shadowed at 45° [S2-604]. Planar cleavage surfaces (A) are separated by steps which are (a) cleaved on oblique planes, (b) parted or (c) conchoidally fractured.

imperfectly crystallographic in texture), or (c) conchoidal. In Figure 8, transition can be observed from cleavages of several types in the lower portion to a more finely textured, wavy, and apparently sheared region near the top.

Some cleavage steps are rich in crystallographic detail, as in Figure 9,* and indicate that conditions comparable to those resulting in cleavage crack segments are also involved in causing the breaks between them. In addition to prominent cleavages, some of the features in this figure are suggestive of twinning. Very fine, directionally aligned texturing shown on these cleavage faces is of particular interest, since it appears to indicate some fine scale plastic working during propagation of the cleavage crack. Very local plastic processes, by causing some blunting of the crack tip, could well account for previously described descrepancies between Bruce's[53] calculated surface free energy for alumina (~ 1057 ergs/cm^2), and Wiederhorn's[55] measured cleavage fracture energies (~ 6000 ergs/cm^2).

Some of the features shown in Figure 10 suggest that certain cleavage steps in finely textured regions may be associated with zones previously sheared, as by deformation twinning. The complex state(s) of stress existing during impact in this anisotropic crystal, coupled with reflections of shock waves, could well account for such sequences of damage.

---

*A direct replication technique (involving (1) angled platinum or platinum-carbon shadowing and (2) normal carbon replica buildup directly on the surface, followed by (3) treatment in HF to facilitate nondestructive chemical release of the replica, as described by Gutshall, et al.,[99] and Gutshall and Shaw[100]) has been adapted for use with sapphire by co-workers on another project. M. L. Huckabee, Graduate Research Assistant, and E. B. Roberts, Laboratory Assistant, made this alternate, very excellent, replication technique available for Figures 9, 10, 11, and 12 of this report. Their cooperation and assistance is gratefully acknowledged.

Figure 8. Transitions from cleaved (lower) to sheared (upper) regions in ballistically damaged sapphire, X15,000.
Two stage plastic-carbon replica, Pt-shadowed at 45° [S2-577].

Figure 9. Fine textures associated with cleavage in ballistically damaged sapphire, X4,800.

Pt-C shadowed direct carbon replica [S11-1333].

Chemically stripped direct carbon replicas are quite brittle, and therefore are very unlikely to generate deformation artifacts. Hence, fine texturing (indicated by arrows) and deformed regions shown in this figure are indicative of localized plastic deformation associated with cleavage crack propagation.

Figure 10. Cleavage fracture across previously sheared regions in ballistically damaged sapphire, X23,300.
Pt-shadowed direct carbon replica [S12-1562].
Arrows mark offsets which suggest that shear resulting from deformation twinning occurred on planes almost normal to the picture plane either prior to or concurrent with cleavage fracture.

Anomalies in an otherwise fairly regular fine cleavage texture are shown in Figure 11. These anomalies may be associated with interactions between the advancing crack front and slip bands or subgrain boundaries pre-existing in the flame grown crystal.[21, 24, 25, 68] Alternatively, such textures may have come about as a consequence of stress field preturbations arising from reflections of shock waves.

Although much of the fracture surface in sapphire is distinguished by sharp angularities, and appears to be characteristic of classical cleavage with little evidence of yielding per se, some portions are suggestive of more generalized deformation that, in comparison, is indicative of localized bulk plasticity. The direct carbon replication fractograph in Figure 12 provides one such example.

A General Consensus for Impact Effects in Sapphire

The combined evidences indicate that single crystal sapphire has relatively low impact resistance, principally because of its predominant, almost catastrophic, cleavage failure modes. Cleavages on a total of four first and second order rhombohedral planes accounted for virtually all the visible and significant crystallographic detail in the specimen studied. At electron microscopic magnifications and resolutions, some evidences of permanent deformation processes were observed, but only on a very local scale. These limited yielding processes, which appear to be capable of blunting or redirecting an advancing crack front, are considered to be consistent with the rather high fracture surface energies ($\gamma_f \approx 6\gamma_s$) reported for rhombohedral cleavage by Wiederhorn.[55]

Figure 11. Abrupt transitions from straight to irregular cleavage steps in ballistically damaged sapphire, X28,400.
Pt-shadowed direct carbon replica [S12-1561]. Two examples are shown along lines A-A' and B-B'.

Figure 12. Transition from cleavage to more generalized plastic deformation in ballistically damaged sapphire, X12,200. Pt-C shadowed direct carbon replica [S11-1388]. By tilting the replica in the goniometer stage, surface details can be examined within pockets from which material has been torn during fracture. This pocket appears to have been subjected to bulk deformation, especially in the upper portion, resulting in flow processes (locally resembling ductile fractures in metals) which modify the dominant cleavage fractures. [Grey specks are impurity artifacts introduced after replication.]

Polycrystalline Alumina

The best available information suggests that damage produced by an impacting projectile in a polycrystalline ceramic occurs in at least four successive stages, with each stage being identified with a particular fracture geometry, stress configuration, and energy spectrum. In an approximate, decreasing order of the total system energy remaining to be dissipated, these stages result in (1) comminuted particulates from within a shear conoid whose axis is the impact trajectory, (2) fracture surfaces associated with the shear conoid interface, (3) radial cracks whose surfaces are approximately parallel with the impact trajectory, and (4) late-phase spall cracks whose surfaces are almost perpendicular to the impact trajectory.

Comminuted material from the first category was not available for this study, but representative replicas of each of the three subsequent stages of fracture were prepared at selected positions as indicated in Figures 2c and 2d. Subsequent sections present microstructural and fractographic information obtained from these replicas.

Conoid Shear Surface

Very little of the principal conoid shear surface was available for study. The replicated surface was obliquely oriented (~ 45°) with respect to the impact trajectory (see Fig. 2d). Figure 13 illustrates several features characteristic of this heavily damaged surface. Fracture was predominantly transgranular, and was rather direct, producing relatively flat, fan shaped river patterns, some of which show multiplications of river pattern components as the fracture front traverses subgrain or grain boundaries.[68] In many instances, progressions from one grain to the next appear to have required considerable shear damage before the crack could be

Figure 13. Complex fractography of conoid shear surface in ballistically damaged polycrystalline alumina tile, X6,900. Two-stage plastic-carbon replica, Pt-shadowed at 30° [D1-386].

freed to proceed ahead in river pattern cleavages or intergranular separations. Within these sheared regions, distinctly localized and heavily concentrated groupings of small bumps or protrusions have been noted. Their origin has not been clearly established, but they appear to suggest deformation processes akin to the early stages of micropore development during plastic fracture in metals.[65-67]

One of the most unique features of this early phase of fracture is the very considerable number of fracture fragments (small, dark shards) which have been extracted *in situ* by the replication process. These fragments suggest that branching and/or multiple cracks[6] were not uncommon at this stage of impact energy absorption. Strong association of fragments with sheared regions suggests that locally intense plastic processes may have played a significant role in their formation. Examinations of some of these fragments in direct transmission have revealed high concentrations of dislocations [this phase of the study is reported in a subsequent section].

Radial Crack Surfaces

Radial cracks apparently begin to propagate during an impact event at a time after the shear conoid has been well established; their formation is probably concurrent with dissipation - by several processes - of a substantial part of the total impact energy. Such cracks tend to propagate perpendicularly outward from the axis of the shear conoid, and extend for considerable distances — as far as the tile edges in the specimen studied.

The first portions of the primary radial cracks are relatively smooth, and are thought to be generally similar in terms of fractography to the conoid shear surfaces described above. The main run of the cracks develop very rough surfaces, with complex textures whose elemental "wave forms" have

amplitudes and periods extending over an estimated 10^2 to 10^3 grain diameters. Final portions of such cracks, especially if diverted or offset, tend to become relatively smooth again.

Figures in this section show fractographic details at three differen radial distances along one radial crack (refer to Fig. 2d). The replica (SD-3) represented by Figure 14 was taken ~ 2.8" from the point of impact in a region of heavy, rough texturing. The next three illustrations come from a replica (SD-4) positioned ~ 3.7" from the center on a more smoothly textured predominantly conchoidal surface produced by the main crack after it had undergone an abrupt offset, then continued approximately parallel to - but with ~ 0.2" displacement from - its original path. The last three figures in this section show surface features on a relatively smooth transverse crack (a secondary crack almost normal to the main crack) at a distance of 3.9" from the point of impact (replica SD-5).

Rough Surfaces. As Figure 14 illustrates, heavily stepped fracturing based on intersections of two first order and one second order rhombohedral cleavage planes constitute one significant fracture mode in the rough portions of radial cracks, just as in the single crystal case previously described. Intergranular separations also have been observed to be quite prominent in the still incomplete investigation of this experimentally difficult fracture category. [Only scanning electron microscopy (combining moderate to high magnification, high resolution, and extreme depth of focus) is likely to provide adequate characterizations of such rugged but finely detailed surfaces.]

Figure 14. Heavy stepped cleavage fractures and intergranular separations on roughly textured portion of a radial crack in ballistically damaged polycrystalline alumina tile, X12,000. Two stage plastic-carbon replica, Pt-shadowed at 45° [SD3-601].

Smoother Radial Crack Surfaces. Though this region was relatively smooth in the macroscopic sense, the replication electron micrographs shown in Figures 15-17 illustrate the extremely complex nature of surfaces produced by highly localized combinations of almost every possible fracture mode. Transgranular conchoidal fracture is more prominent than in the previous examples. The curving conchoidal fractures are neither smooth nor uniformly textured. Rather, they contain an abundance of fine detail which suggests that the advancing crack was sensitive either to progressive changes in crystallographic orientation, or in local states of stress and strain, or both. Very high surface energies ($\gamma_f \geq 40{,}000$ ergs/cm^2) were associated with non-planar fracturing (i.e., conchoidal in character) in attempts to cleave basal planes in sapphire.[55] The conchoidal surfaces illustrated here appear to provide many evidences of real resistance to separation. In comparison to essentially brittle cleavages, they appear to have been produced by cracks which had been subjected both to some blunting and to continuous redirection. Such textures are probably not inconsistent with very large fracture surface energies.

In Figure 15, conchoidal fractures, intergranular separations, two very characteristic forms of rhombohedral cleavage, and several examples of fracture fragment formation are illustrated. The central grain shows a very well defined shift from intergranular separation to transgranular cleavage. A similar case is shown near the center of Figure 16, where a small, relatively featureless region of favorably oriented grain boundary separated to advance the crack, but was surrounded by transgranular conchoidal fractures which were locally modified by cleavage and/or parting. In Figure 17, the long central boundary surface shows another transition from boundary separation on the right (which grades off into parting and conchoidal

Figure 15. Intergranular separations, transgranular cleavage steps, conchoidal fractures and *in situ* fracture fragments contribute to the very complex topography of a smoothly textured portion of a radial crack in ballistically damaged polycrystalline alumina tile, X9,600. Two stage plastic-carbon replica, Pt-shadowed at 30° [SD4-382].

Figure 16. Fracture fragments and transition from intergranular separation to transgranular fracture on a smoothly textured portion of a radial crack in ballistically damaged polycrystalline alumina tile, X9,600.
Two stage plastic-carbon replica, Pt-shadowed at 30° [SD4-378].

Figure 17. Transition from intergranular separation to transgranular fracture along grain edge junction on a radial crack surface in ballistically damaged polycrystalline alumina tile, X9,600. Two stage plastic-carbon replica, Pt-shadowed at 30° [SD4-379].

fracture) to transgranular fracture on the left. Of particular interest is the strong redirection of the transgranular fracture (just to the left of the boundary trace) together with the unusual sheared appearance at the left of the boundary flat. Such a configuration possibly is associated with some grain boundary sliding[43] at a constrained triple grain edge, causing a small amount of shear. Relaxation of the strains imposed would require either generalized plastic deformation or transgranular fracture of one or more of the adjacent grains.

Smooth Transverse Fractures. The surface studied in Figures 18-20 is considered to be a secondary crack (possibly a consequence of reflected stresses) and may be representative of a somewhat later portion of the fracture time sequence and a proportionally lower segment of the energy dissipation spectrum. The principal fracture features include both grain boundary separations and transgranular breaks, together with generation of fine fracture fragments. The transgranular portions range in texture from conchoidal to imperfect parting to well defined cleavage. The orthogonally stepped cleavage mode commonly observed on single crystal fracture surfaces and on primary radial cracks in this polycrystalline material is less evident in this secondary crack. The intensity of texturing is significantly reduced from the more severe cases previously cited (compare Figures 5-9, 14, and 15 with 18 and 20).

At the higher magnification of this surface provided by Figure 19, there are several interesting examples of interactions between the advancing crack and the crystalline substructure (principally subgrain boundaries). These interactions apparently result in very local alterations of the fracture texture, as noted by Low.[68]

Figure 18. Fracture textures on transverse secondary crack in ballistically damaged polycrystalline alumina tile, X9,600. Two stage plastic-carbon replica, Pt-shadowed at 30° [SD5-402].

Figure 19. River pattern cleavage steps on transverse secondary crack in ballistically damaged polycrystalline alumina tile, X31,200. Two stage plastic-carbon replica, Pt-shadowed at 30° [SD5-391]. Multiplications and redirections occur at the grain boundary marked by line A-A'; other changes along B-B', C-C', D-D', D'-D'', and B'-D' may be indicative of the influence of subgrain broundaries. Arrows indicate local directions of advancing crack.

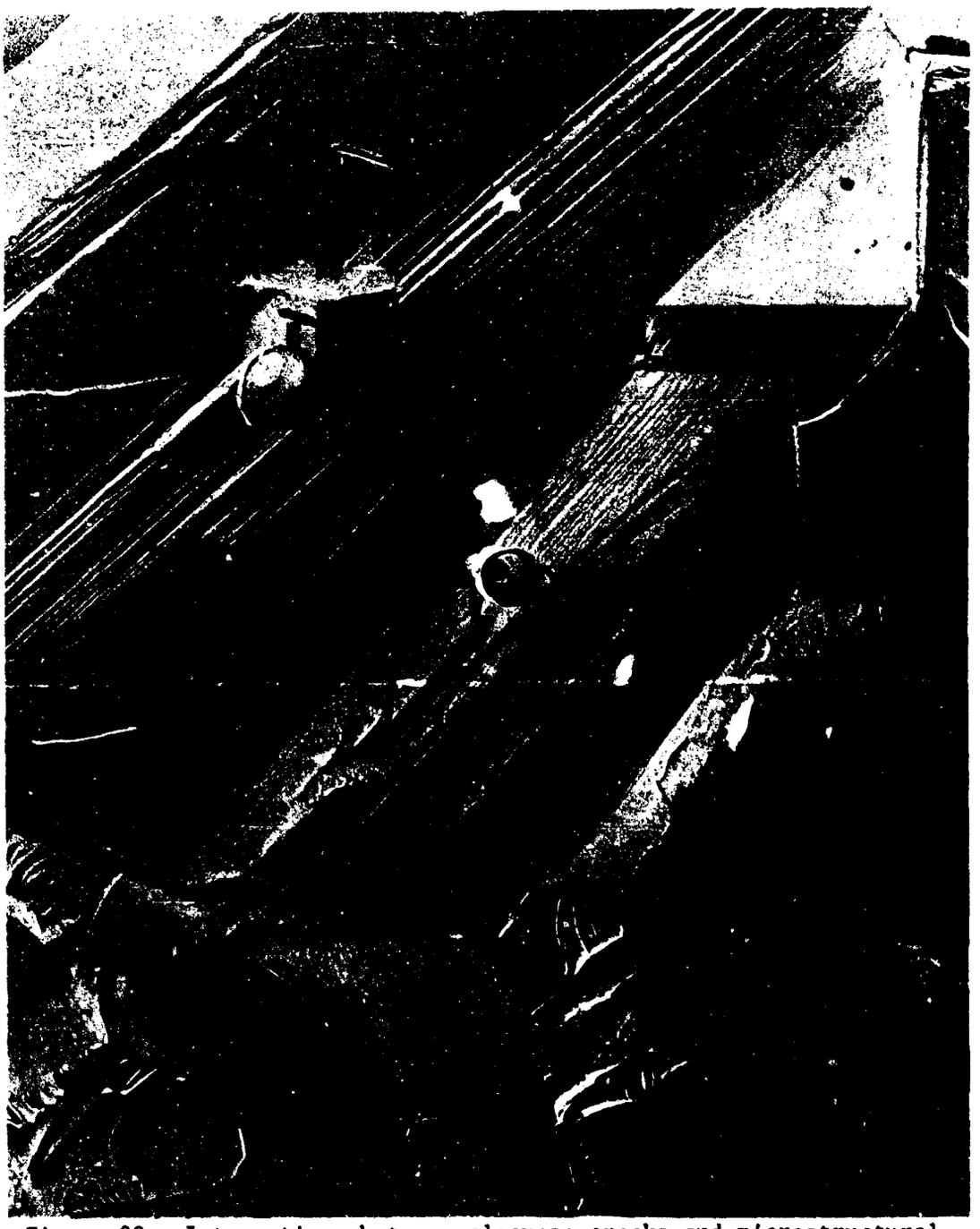

Figure 20. Interactions between cleavage cracks and microstructural features on transverse secondary crack surface in ballistically damaged polycrystalline alumina tile, X9,600.

Two stage plastic carbon replica, Pt-shadowed at 30° [SD5-404]. Letters A through F identify grain boundaries, pores and fracture details discussed on p. 56.

Figure 20 provides some interesting examples of interactions between advancing cleavage cracks and microstructural features. Angular grain boundaries (A) at the upper right are typical of polyphase ceramic bodies which rely in whole or in part upon liquid phase sintering.[101-103] The crack was not significantly altered in perpendicularly traversing these thick and presumably vitreous boundaries, but cracks running within other, differently oriented thick boundaries might be expected to produce hackled, splintered and/or conchoidal textures typical of fracture in glassy materials.[104]

After changing from boundary separation to transgranular fracture at (B), the crack produced finely textured but very irregular stepped cleavage fractures in moving toward pore (C). Since the nearby - and nearly parallel - grain boundary (D) appears to have been separated, it may be that these cleavage anomalies result from stress relaxation associated with the separated boundary coupled with normal resistance to cleavage within the grain and at its other boundaries.

At the pore (C) several changes in fracture behavior can be noted, both in the immediate pore vicinity, and at longer distances extending to the end of the grain. Related fracture tails at microstructural discontinuities in ceramics and glasses have been reported elsewhere.[59, 105]

The downstream tailing effect is less prominent for the faceted pore (E), but the pore possibly did cause the unusual cleavage perturbations oriented in a perpendicular direction at (F). The discontinuity represented by the pore may have caused stresses associated with the crack front to be resolved into new components, including those capable of producing this anomaly.

Late-Phase Spall Cracks

This category of fracture damage, though prominent in terms of total exposed area (see Fig. 2b and 2c), is thought to be representative of the final stages of cracking, occurring at a time when the kinetic energy of impact has been substantially dissipated. Both transgranular and intergranular fracture modes are observed. In Figures 21 and 22, cleavage is the most characteristic process for transgranular fracture, but the roughness of texturing produced by cleavage is not as severe as in the earlier fracture stages in this material or in the previously described single crystal. Significantly, there is very little evidence of fracture fragments of the sort which were common on more severely damaged surfaces.

Comparisons of Impact Fracture with "Slow" Fracture

One large segment of the broken polycrystalline alumina specimen was cut with a diamond saw into test specimens which measured (after diamond grinding) 0.343" x 0.085" x > 1.5". These specimens were broken in four point bending in a test fixture described elsewhere.[59] The calculated outer fiber tensile strengths, which are fairly typical for this commercial grade of alumina, are shown in Table II.

Table II. Single Stroke Bend Strength of Polycrystalline Alumina After Exposure to Ballistic Impact.

Specimen	Behavior	Outer Fiber Tensile Strength*
1	Strong	30,420 psi
2	Strong	32,950
3	Strong	35,440
Average of "strong" specimens		32,936
4	Weak	17,550

*Four point bending, one inch span. Crosshead strain rate 0.02 in/min.

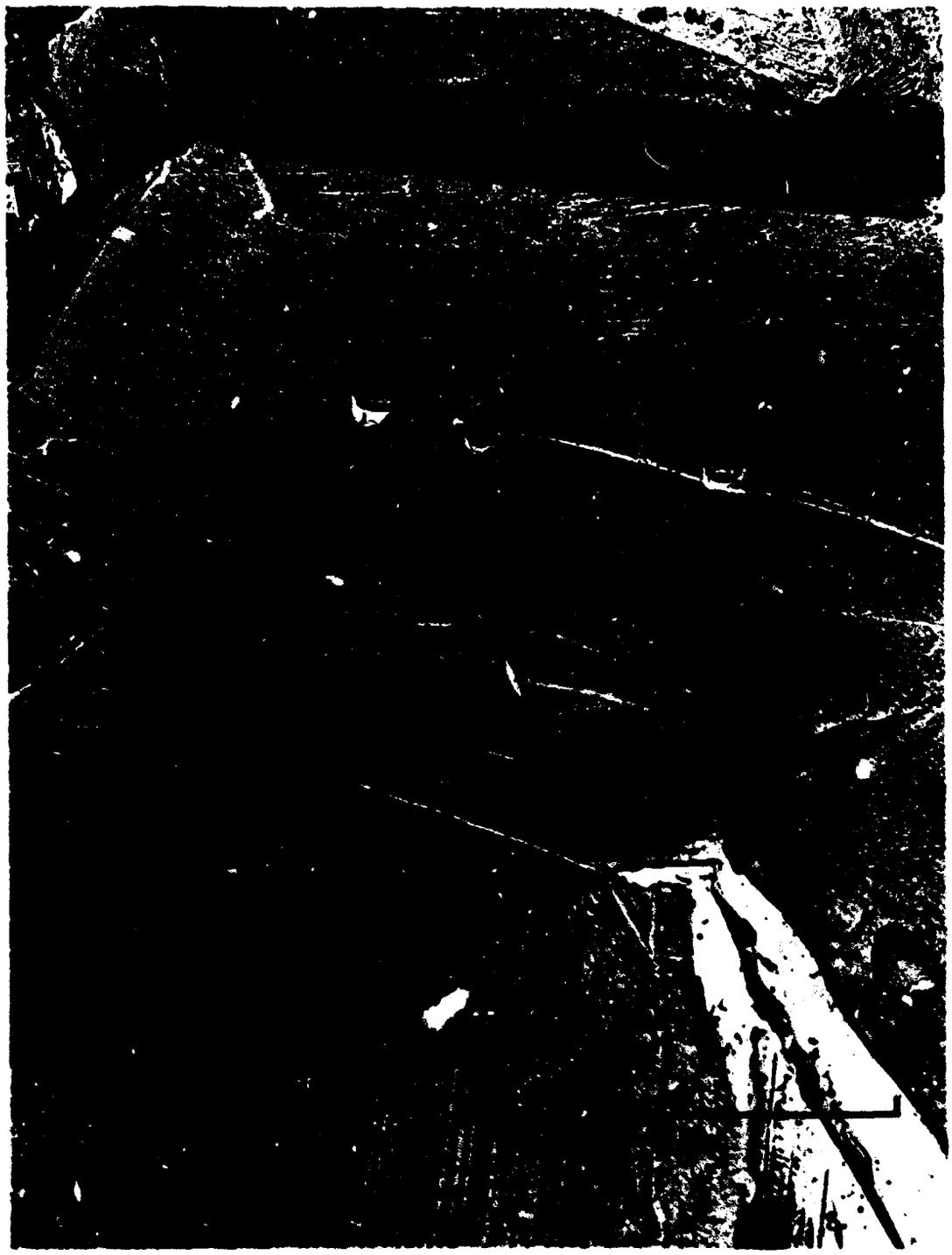

Figure 21. Intergranular separations and transgranular fractures on late-phase spall crack surface in ballistically damaged polycrystalline alumina tile, X13,850.
Two stage plastic-carbon replica, Pt-shadowed at 45° [A1-331].

Figure 22. Transgranular cleavage fracture on late-phase spall crack surface in ballistically damaged polycrystalline alumina tile, X21,500.
Two stage plastic-carbon replica, Pt-shadowed at 45° [A3-328].

Replication fractographic studies of these slow break fractures show surprisingly few differences in comparisons with the impact produced fractures described in earlier sections. The typical surface shown in Figure 23 demonstrates cleavage, parting, and conchoidal transgranular fracture modes along with some intergranular separations. Fracture fragments were extracted *in situ* by the replication process [some have been examined in transmission and show evidences of deformation, as discussed in a subsequent section].

Interpretations of these ambient temperature bend tests and resulting fracture features must take into account the prior exposure of the material to severe shock waves during impact. One could argue that the fracture details are more likely to be the result of damage produced during impact, rather than during the subsequent bend test. However, some of that argument can be refuted by noting many similarities between these data and fractographic details observed in single break double cantilever fracture energy specimens of polycrystalline alumina by Gutshall *et al*,[99] and by citing the recent observation by Congleton, et al,[107] of dislocation densities of ~ $10^9/cm^2$ in transmission electron microscopic studies of fracture fragments produced by single stroke breaks at ambient temperature in bent crystals of α-Al_2O_3 and in alumina ceramics.

Evidences of Fracture-Induced Plastic Deformation as Revealed by Transmission Electron Microscopy

Replicas of the conoid shear surface of the polycrystalline alumina armor specimen contained many fracture fragments (see Fig. 13). Some of them were thin enough to permit reasonably effective study of internal defects by direct transmission electron microscopy at an accelerating potential of 120 Kv. This section of the report presents a rather detailed study of

Figure 23. Fragments, intergranular separations, transgranular cleavage steps, and multiplications of river patterns on fracture surface resulting from four-point bending of rectangular bar cut from ballistically damaged polycrystalline alumina tile, X12,000. Two stage plastic-carbon replica, Pt-shadowed at 30° [SRF1-493].

heavy concentrations of dislocations one such fragment.* Similar (though not such well documented) defects are also shown to occur in impact-produced fragments from a single crystal specimen, and in fracture fragments produced by bend testing of polycrystalline alumina at slow loading rates.

Fragment from Conoid Shear Surface

The fragment in question is shown on the replica in Figure 24, together with other generally similar but less transparent fragments. In this instance, damage to this region of the replica makes it impossible to ascertain whether or not the fragment was picked up at the place of origin. However, the preceding replication fractographs make it clear that many, perhaps most, such fragments have been extracted in situ. The fragment is about 2.88μ long, 2μ wide, and variable in thickness, ranging from vanishingly thin edges to the almost opaque center, estimated as $\geq 0.5\mu$. Transmission of the electron beam also was affected adversely by platinum and carbon which had been vapor deposited during the replication process.

Figures 25 - 27 show the relative placements of dislocations at somewhat higher magnification, and with sequential small changes in specimen tilt angles as required to achieve the necessary contrast effects. In Figure 25,† those marked A and A' are very near thin edges, and may have been directly associated with the branching and/or intersecting cracks

---

*Dr. R. B. Benson, Jr., Associate Professor of Metallurgical Engineering, assisted in obtaining and interpreting many of the transmission electron micrographs. P. F. Becher, Research Associate, developed reciprocal lattice reference data for α-Al_2O_3, and indexed the electron diffraction patterns which have been identified to date. Their assistance has been invaluable, and is gratefully acknowledged.

†Thickness variations in this specimen create many problems in providing adequate photographic contrast for the details of interest. Figures 25a and 25b were enlarged from the same plate, under different contrast conditions. Contrast in Figure 25a has been adjusted to resolve the edge details, but has been shifted in Figure 25b (and in subsequent Figures) to emphasize the interior dislocations.

Figure 24. Fracture fragments from conoid shear surface in ballistically damaged polycrystalline alumina tile, X24,000.
Extracted fragments on two stage plastic-carbon replica, Pt-shadowed at 30° [D1-1842].
At 120 kV (rather than the 80 kV normally used in replica studies) portions of the bulkier fracture fragments can be examined in direct transmission. Arrow identifies one such fragment selected for detailed study in Figs. 25-30.

a. Photographic contrast adjusted to reveal edge details.

Figure 25. Locations of structural defects in fracture fragment from conoid shear surface in ballistically damaged polycrystalline alumina tile, X75,000.
Extracted fragment on plastic-carbon replica, Pt-shadowed [D1-1813].
Letters locate dislocations and other features described on pp. 62 and 68.

b. Photographic contrast adjusted to reveal interior dislocations.

Figure 25, continued.

Figure 26. Same fragment, tilted to slightly different orientation to achieve stronger contrast on interior dislocations, X75,000. Extracted fragment on plastic-carbon replica, Pt-shadowed [D1-1815]. Shifting away from a Bragg diffraction condition (which caused overall darkening in Fig. 25) permits more of the transmitted beam to penetrate good portions of the crystal, thereby enhancing visibility for dislocations along A'-D and C-D. However, those along C-E have lost contrast. Lattice distortions around dislocations can either re-establish or further diminish Bragg diffraction conditions in small adjacent regions. These contrast effects make imaging of dislocations possible.

Figure 27. Additional tilting of the fragment (for two beam diffraction) reduces contrast for dislocations previously imaged, but brings a very densely populated region along C-E into strong contrast, X80,000.
Extracted fragment on plastic-carbon replica [D1-1823].

which separated this fragment from the bulk. Similarly, those approaching the fragment boundaries at C, D, and E in this figure probably have a functional relationship with either or both of the two cracks which formed the thin edges. In somewhat thicker material at the locations marked B and B' - curving dislocations can be seen which appear to be either complete (B) or partial (truncated) loops (B'), generally similar to grown-in defects shown in sapphire single crystals by Barber and Tighe.[83] The intersecting group of dislocations at C appear to be relatively broad and ribbon-like, and display a variety of contrast effects at their intersections. Such characteristics are typical of extended dislocations which have been examined in other materials.[106, 108] The dislocations pictured here have not yet been subjected to detailed analysis, but it is pertinent to note that such extended dislocations, if confirmed, might not be inconsistent with Kronberg's[109] quarter-partial synchroshear model for basal dislocations in α-Al_2O_3.

A number of more or less parallel individual dislocations make up a band along the line A'- D. Curving and interacting dislocations make up another band along the line C - D. A separate and densely populated group, out of contrast in Figures 25 and 26, but in contrast in Figure 27, occurs along the line C - E. Finally, a well defined Y-junction is visible at F.

Figure 28 was obtained at higher magnification after the specimen had been tilted to another orientation (a two beam diffraction condition) producing well defined linear traces for dislocations in the A - D and C - D groups, but no contrast for the C - E group. Additional tilting to another two beam diffraction condition yielded the bright field image shown in Figure 29, in which the A, A', B, B' dislocations have no contrast, while those along A' - D, C - D, and at F have weak contrast, appearing as single lines.

Figure 28. Another two beam diffraction case provides additional detail of A'-D and C-D dislocations in thickest portion of fragment, X120,000.
Extracted fragment on plastic-carbon replica [D1-1840].
[Spots are artifacts associated with flaws in plate emulsion.]

Figure 29. Additional information about dislocations is provided by different contrast conditions available from another orientation selected to yield two beam diffraction, X120,000
Extracted fragment on plastic-carbon replica [D1-1847; inset 1845]. The $\bar{g}$ vector (arrow in inset diffraction pattern) describes crystallographic relationships between transmitted beam and the strong diffracted beam responsible for these dislocation contrast effects. Diffraction pattern also identifies this picture plane as the $(2\bar{1}\bar{1}0)$ prism plane.
Note: electron diffraction data are most easily described in terms of the structural unit cell, c/a = 2.730:1. Figures 29 and 30 have been indexed in structural notation, and hence differ from morphological indices used elsewhere in this report.

Subsequent tilting to yet another orientation for two beam diffraction produced strong contrast for dislocations concentrated along the line C - E, and a related set near D, as shown in Figure 30. The A, B, A'-D, C - D, and F sets of dislocations shown earlier either were not in contrast, or were only weakly visible. Detailed evaluations of these recent data are not complete, but sufficient information apparently has been obtained to permit complete identifications of the pertinent slip systems in the near future. Though analysis is incomplete, the findings are well enough established to warrant these significant general comments.

1. It is likely that two, perhaps three, different slip systems have been involved in producing the imaged dislocations.
2. The dislocations are concentrated in bands which appear to bear appropriate geometric relationships with the kinds of shearing actions which are likely to have been taking place as the fragment was being torn from the bulk.
3. The dislocation densities within these sheared zones are quite high. In some high density regions, the separation distances are $\leq$ 350Å, i.e., only 25 - 30 structural c_o units apart. The local dislocation density has been estimated to be at least $8 \times 10^{10}/cm^2$. This value is approximately five orders of magnitude larger than those reported for grown-in dislocations in flame grown sapphire crystals.[21, 23-25]
4. Very significant quantities of energy have been absorbed by plastic deformation occurring prior to and/or during fragmentation. This excess energy has been retained within the structure of the fragment, and is concentrated in high energy lattice distortions associated with each of the many individual dislocations.

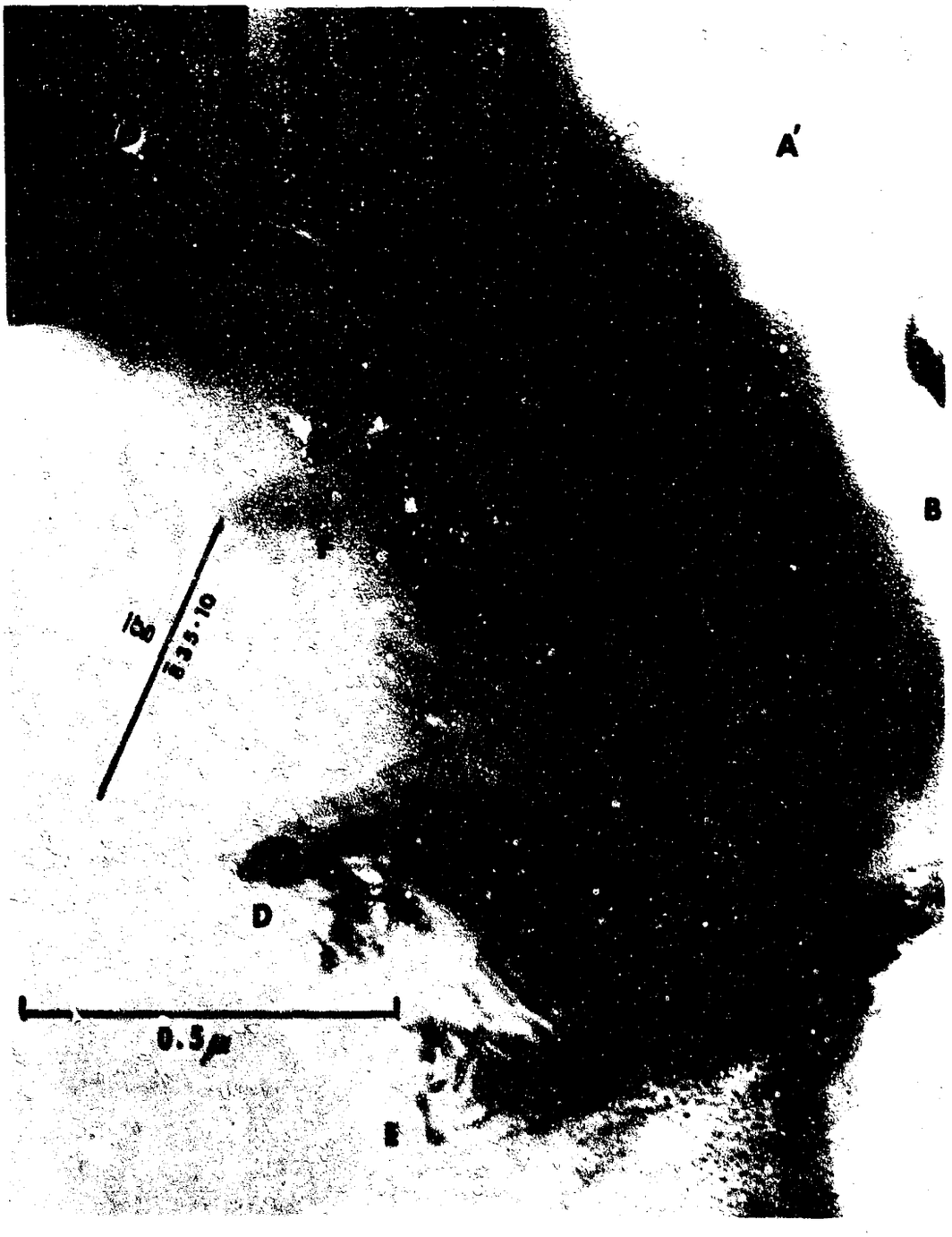

Figure 30. Bright field image with two beam diffraction for $(03\bar{3}3)$ orientation in fragment from conoid shear surface in ballistically damaged polycrystalline alumina tile, X120,000.
Extracted fragment on plastic-carbon replica [D1-1836; inset 1834].
Compare with different contrast conditions in Figs. 28 and 29.

Fragment from Single Crystal Cleavage Surface

Occasional fracture fragments were observed in examining direct carbon replicas of ballistically damaged sapphire single crystals (Refer to Figs. 10 - 12). One such fragment was examined briefly in direct transmission, with the results shown in Figure 31.* A crack enters at A and appears to terminate within the fragment at B. The crack terminates at B in a region of high contrast which, though poorly resolved, appears to have mesh-like character not unlike a subgrain boundary made up of screw dislocations.[85,106] Other bright field and dark field views obtained under different tilt conditions -not illustrated- tended to confirm this observation. Parallel lines at C suggest that twinning may have provided additional deformation. In some locations, as at D, the thin edges show contrast effects indicative of defects. Similar observations of dislocations (~ $10^9/cm^2$) in fragments produced during simple breaking of bent sapphire single crystals and alumina ceramics have been reported recently by Congleton, et al.[107] †

---

*This figure has relatively poor quality in comparison with those preceding it; experimentalists may wish to note the reason for the difference. A principal factor is thought to be a rather rapid deterioration of the specimen in Figure 31 due to progressive contamination (build up of carbonaceous deposits) under the influence of electron irradiation within the microscope. Electron beams of low intensity are sufficient for replication fractography at modest magnifications, and anti-contamination cold trapping with liquid N_2 normally is not required. At the higher magnifications and more intense beam currents needed for direct transmission, contamination effects become quickly apparent if trapping on a cold surface is not employed. Without the protection provided by the anti-contamination trap, the fragment in Figure 31 was almost completely obliterated in ~ 30 minutes. By comparison, and with proper trapping, the fragment shown in Figures 24 - 30 remained in good condition for more than eight hours of total exposure to an electron beam of comparable intensity.

†Their very significant paper, which confirms the principal findings and conclusions of the present study, and warrants much further discussion, did not become available until this report was essentially complete.

Figure 31. Defects in fracture fragment from ballistically damaged sapphire crystal, X31,000.
Extracted fragment on direct carbon replica, Pt-shadowed [S11-1368].
Letters locate features described on p. 73.

Fragment from Slow Break Fracture in Polycrystalline Alumina

Fracture surfaces resulting from single stroke bend tests of polycrystalline alumina bars contained a number of extraction fragments (see Fig. 23). [Similar fragments can be seen in Gross and co-workers' [8, 99, 110] replication fractographs from double cantilever fracture energy specimens of polycrystalline alumina.] Several of the fragments from this study have been examined by direct transmission, and many evidences of defect structures have been observed. One such fragment - not oriented for optimum contrast - is illustrated in bright field in Figure 32, and another fragment is shown in dark field in Figure 33. The dislocation densities are nearly comparable with those in impact fragments.

Such evidences of plastic work contributions to ordinary fracture processes in α-Al_2O_3 are consistent with X-ray evidences reported by Guard and Romo[111] of residual strain which they attributed to very shallow plastic flow zones associated with crack surfaces in sapphire single crystals and polycrystalline alumina ceramics. These evidences of plasticity operative during fracture of this nominally brittle material also indicate that significant quantities of plastic work may be contributing to the abnormally high fracture surface energies (~ 25,-00 - 50,000 ergs/cm^2) measured in polycrystalline alumina by Clarke, et al.,[6] Congleton and Petch,[54] and by Swanson and Gross.[110]

Excess Energy in Explosively Shocked Alumina Particulates

As a [temporary] substitute for comminuted material from within impact-produced conoid regions, explosively shocked Linde A alumina has been examined for evidences of residual strain energy by dynamic differential calorimetry. These particulates also have been compared with the unshocked control sample by electron microscopy.

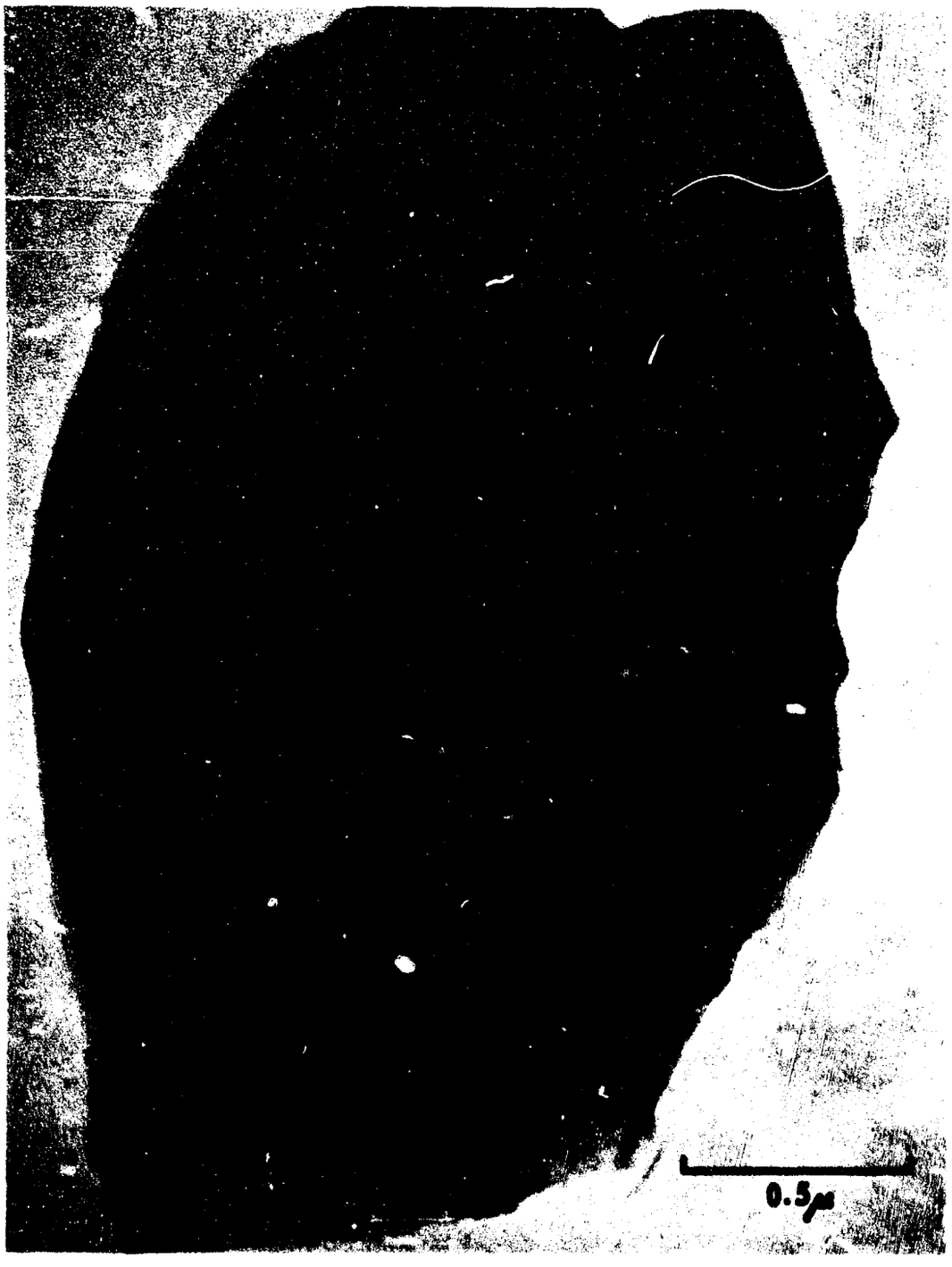

Figure 32. Bright field image of defects in fracture fragment from single stroke break in bar cut from ballistically damaged polycrystalline alumina tile, X72,000.
Extracted fragment on plastic carbon replica, Pt-shadowed [SRF1-459].
Compare with dark field image of another fragment from same surface (Fig. 33), and with impact-produced fragment (Figs. 25-27).

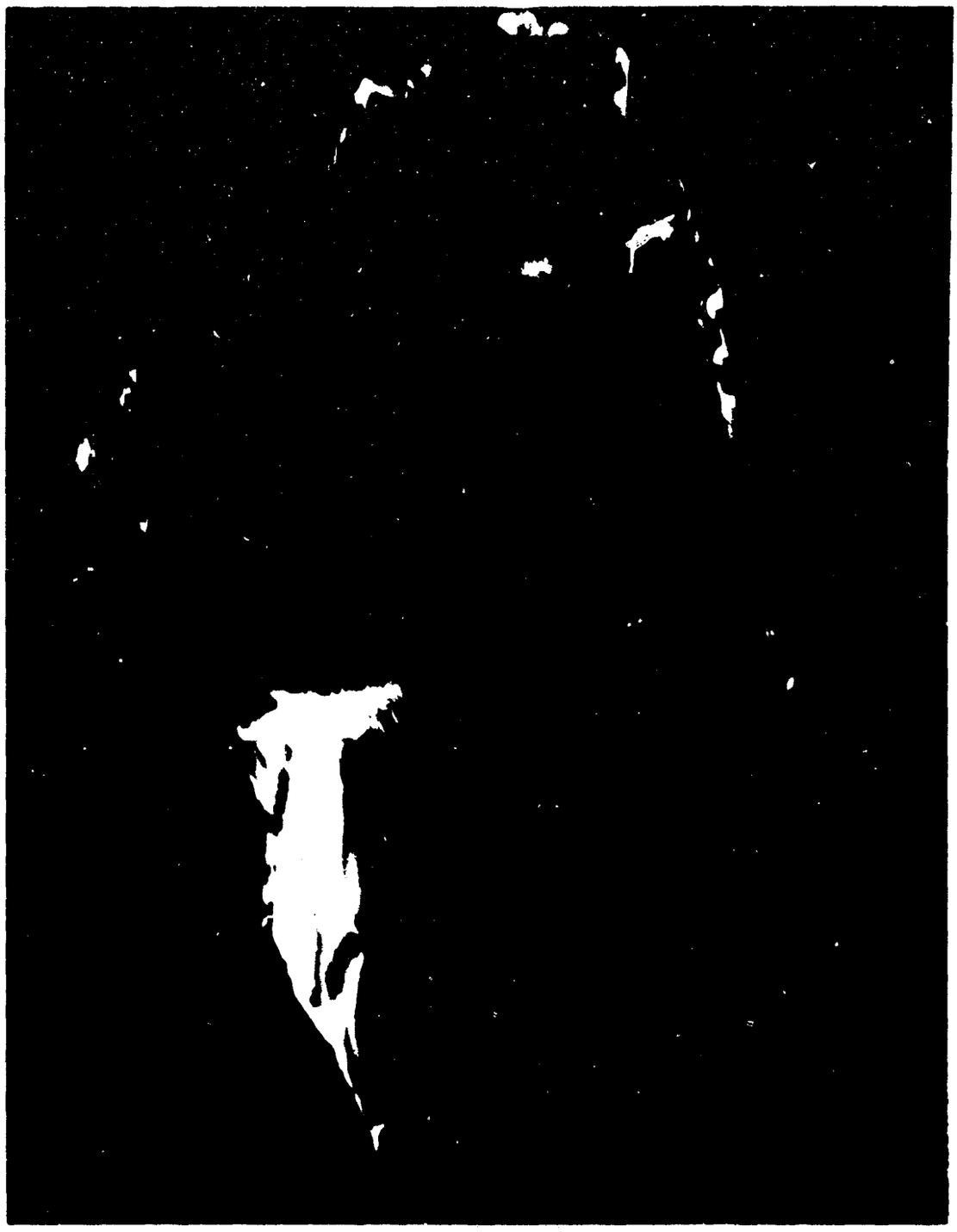

Figure 33. Dark field image of defects in fracture fragment from single stroke break in bar cut from ballistically damaged polycrystalline alumina, X48,000.
Extracted fragment on plastic-carbon replica, Pt-shadowed [SRF1-525]. In dark field electron microscopy, the illuminating electron beam is selectively tilted out of view; a strong diffracted beam is centered to produce the image. Therefore, light images correspond to regions at and around defects which have enough local distortion to tilt the lattice to the necessary Bragg diffraction condition.

Microstructure of Particulates

The control material (Fig. 34) contains two phases. The dominant α-Al_2O_3 final product has irregular, rounded, often protuberant shapes, while the intermediate, metastable γ-Al_2O_3 minor phase is extremely fine grained and flocky.*

After explosive shocking at particle velocities in the 300 - 1000 in/sec range,[48] the material was found to be significantly altered (Fig. 35). The γ-Al_2O_3 particles were deflocculated and dispersed, and some of the α-Al_2O_3 particles had been fractured in neck regions. In direct transmission,† many of the α-Al_2O_3 grains showed evidences of defect structure resulting from deformation, including dislocation contrast effects and/or regions of twinning.

Characterization of Excess Energy by Dynamic Differential Calorimetry

Figure 36 is a plot of dynamic differential calorimetry traces over the range 700 - 1200°C for an unshocked alumina control specimen [compared with sapphire] and for three different experiments with shocked alumina [compared with three different reference specimens: (1) sapphire, (2) unshocked control material, and (3) triply annealed shocked alumina].

The sapphire reference is considered to have no latent heat effects over the 20 - 1200°C heating range, but both the unshocked control and the

---

*The reported findings were independently obtained, and are in very good agreement with the manufacturer's published descriptions of this material.

†These rounded grains are too variable in thickness for very effective dislocation studies by transmission microscopy. To obtain acceptable contrast and depth of focus, these plates were exposed at low magnifications, then enlarged photographically.

Figure 34. Linde A alumina powder as received, X60,000.
Deposited on carbon support film as ultrasonically agitated suspension in acetone [PDQ2-1399].
This is the unshocked control material. Compare with explosively shocked Linde A in Fig. 35.

Figure 35. Explosively shocked Linde A alumina powder, X60,000. Deposited on carbon support film as ultrasonically agitated suspension in acetone [PDQ1-1398].
Large γ-Al_2O_3 flocks have been broken and dispersed. Some neck-growth regions in α-Al_2O_3 grains (indicated by arrows) have been broken. Asterisks locate contrast effects considered to be sites of shock-ipduced imperfections in several different α-Al_2O_3 grains.

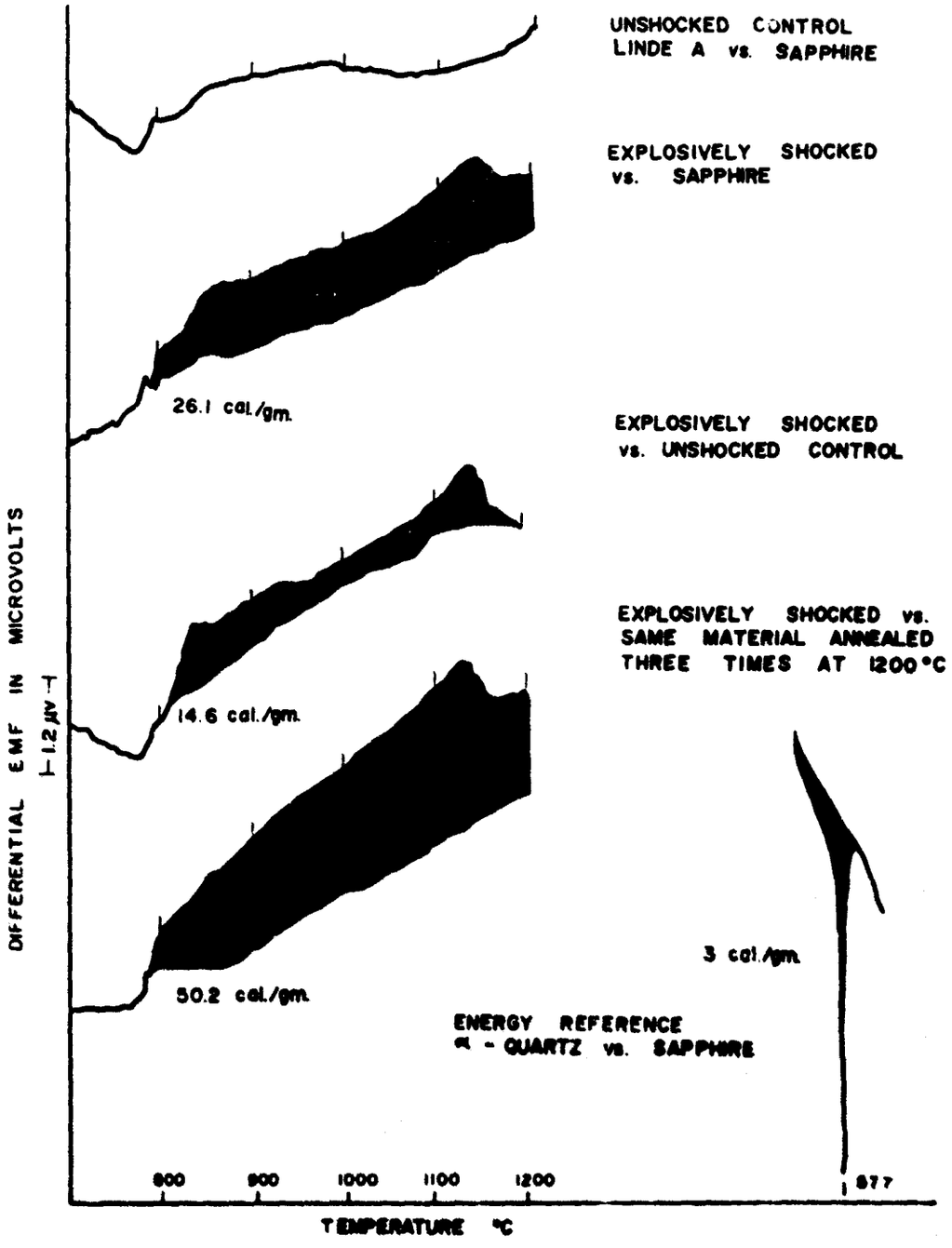

Figure 36. Dynamic differential calorimetry of explosively shocked Linde A alumina powder. These curves, and their tentative interpretations, are described on pp. 78, 82, and 83.

triply annealed material are likely to undergo phase transformations and/or sintering within this temperature span, and cannot be considered to be inert.

In these plots, the solid curves represent the measured differential EMF's obtained as small pressed pellets (closely matched in weight, ~ 150 mg) of sample and reference materials were being heated - for the first time - at a rate of ~ 10°C/min in shallow platinum vessels in a special ring-type differential thermocouple (see p 27). The lower edge of the shaded region beneath each curve for shocked alumina represents the trace of the baseline. The baseline is somewhat temperature dependent, and was determined by repeating the heating cycle a second time without disturbing the specimen holder. Baseline curves have been adjusted vertically - slightly - to provide a normalizing coincidence with the upper curve. Normalizing has been based upon establishing an arbitrary zero difference in EMF between test and baseline runs at a small inflection point (which is characteristic of all runs with this specimen holder) just below 800°C.

The area of the shaded region is amenable to direct measurement by planimeter methods, and may be considered to be proportional to the total exothermic release of energy during the first heating to 1200°C.
To provide a [tentative] reference standard for scaling the energy quantities involved, a plot of the endothermic α to β quartz inversion peak has been included. The energy required for this transformation has been variously reported as 2 - 4 cal/g.[92] For the purposes of this report, the value arbitrarily has been considered to be 3 cal/g.

Plots for shocked alumina - regardless of the reference material selected - consistently indicate a broad exotherm over most of the range above 800°C, with two - or more - characteristic peaks, of which the one at ~ 1130°C is the most prominent. These peaks do not occur in the control

specimen, nor do they recur during second heating runs for shocked material. It seems clear that these exotherms represent - in part - significant releases of energy associated with the annealing of shock-induced strains. However, they are not unambiguous, because other reactions, also exothermic, are considered to be highly likely within this temperature range. They include (a) annealing of strains in the γ-Al_2O_3 second phase (b) transformations of γ - to α-Al_2O_3 and (c) sintering [resulting in a reduction of total surface energy] of α-Al_2O_3. Unambiguous characterization of specific energy profiles associated with annealable excess energy per se will require deformed monophase particulate material free of the confounding effects noted here. These effects, particularly the sintering, are considered to account for significant fractions of the substantial energy differences denoted by the shaded areas.

These preliminary results demonstrate the effectiveness of the DDC method in sensing stored energy effects in shock-modified alumina particulates. [Even greater effectiveness is expected for impact-altered fragments.] The quantities of energy released, even in the most conservative case (shocked vs unshocked), are very substantial (~ 14.6 cal/g. These results are considered to be in excellent agreement with the earlier findings of Bergman and Barrington[48] and Heckel and Youngblood,[49] about enhanced sinterability attributable to strain effects in shocked alumina. This phase of the study also provides substantiation for the importance of densification contributions attributable to annealable excess energy - the "little q" term in the temperature dependent factor $e^{-\frac{(Q-q)}{RT}}$ - contained in a kinetic model proposed by Palmour, et al.,[50] for sintering and/or stress-assisted densification.

SUMMARY AND CONCLUSIONS

Preceding sections of this report have presented mutually supporting and very strong evidences of significant amounts of plastic deformation and energy absorption associated with fracture processes in aluminum oxide ceramics and single crystals. Effects of ductility associated with fracturing have been observed in slow cracks resulting from single stroke bend testing in ambient environments, as well as in those produced under very severe ballistic impact conditions. Comparable levels of structural alteration also have been observed in explosively shocked particulates.

The almost inescapable conclusion to be drawn from these findings is that truly brittle cracks - those which can be propagated with fracture surface energy (γ_f) comparable to the calculated surface free energy (γ_s) without doing work upon the bulk of the material traversed - are relatively rare in this refractory oxide. Rather, the fractures commonly observed in aluminum oxide were propagated (at least in part) as almost ductile or blunted cracks - those in which the fracture surface energy (γ_f) has been substantially increased above the nominal free energy (γ_s) because of plastic work energy (γ_p) which had to be expended in deforming bulk material at and near the advancing crack front.

Fracture surface energies in alumina ranging from approximately 25,000 to 50,000 ergs/cm^2 have been reported by several investigators. Numerical values generally have been based upon calculations incorporating only the projected crack surface area.[6] Actual surface areas have been considered to be as much as three times greater than projected areas,[6] an estimate which is considered to be realistic in terms of the fractographic examinations made during the present study. If the reported gross

values for γ_f are normalized with respect to actual surface areas [i.e., divided by the suggested factor of three], the range for resultant net fracture surface energy (γ_{f_o}) is from approximately 8,350 to 16,700 ergs/cm^2. The net values are some seven to fifteen times larger than calculated surface free energy values ($\gamma_s \approx 1136$ ergs/cm^2).[53] For polycrystalline alumina of moderate grain size, these rather conservative estimates [$\gamma_p = \gamma_{f_o} - \gamma_s$] yield γ_p values ranging from about 7200 ergs/cm^2 to more than 15,000 ergs/cm^2. The Orowan criterion for a plasticity component in fracture, $\gamma_p > \gamma_s$, seems well satisfied.

Microscopic evidences from replication fractography, and particularly from direct transmission electron microscopy, strongly support the concept of localized plastic deformation processes associated with fracture. Dislocation concentrations observed in thin fracture fragments ($\sim 10^9 - 10^{11}$/cm^2) are several orders of magnitude higher than those normally encountered in unworked ceramic materials ($< 10^6$/cm^2) and approach densities ($\sim 10^{12}$/cm^2) which are typical of extensively worked metals.

These results are documentary in character. The present levels of strength and characteristic fracture modes of present grades of ceramics have not been altered by these findings. However, by demonstrating that crystalline plasticity is a concomitant part of the fracture process, they do provide some very different directions by which the present understanding of strength and fracture in ceramics and other nominally brittle materials can be advanced.* To bring them into perspective, it is necessary to speculate about future trends. Such speculative forecasts are embodied in the concluding statements which follow.

Detailed interpretations of the nature of the observed dislocations and other structural defects, and quantitative documentations of their roles in

---

*Parker's March, 1960 comments on this point are still significant.[112]

providing energy absorbing and storing mechanisms will take time, and must be reserved for the future. Predictably, these fundamental aspects of the present findings will be subject to - and will benefit from - rigorous scrutiny within the materials science community.

However, it may not be necessary - or even prudent - for engineering advances to wait upon final, rigorous documentation of the scientific details of the processes involved. Even now, one can accept the reality of demonstrable ductility accompanying fracture in nominally brittle ceramic materials. Thereafter, it will be worthwhile to accept the challenges of learning to take full advantage of this new knowledge.

Dislocation concepts predictably will be employed in (a) developing effective analytical treatments of fracture and strength in almost (but not truly) brittle materials, (b) improving the properties of existing ceramic materials, and (c) fostering the rational development of new ceramics and ceramic-based composite materials. As correlations of pertinent characterization parameters [e.g., dislocation mobility] with compositions and process variables are established, it is probable that useful properties can be enhanced either by optimizing - or minimizing, as the case may be - the limited, yet important, contributions made by plastic flow and stored energy to kinetics and mechanical behavior in crystalline ceramic substances.

Acknowledgements

Dr. R. B. Benson, Jr., P. F. Becher, M. L. Huckabee, E. M. Gregory and E. B. Roberts provided valuable technical assistance in experimental phases of this research, and made substantial contributions to the interpretation and presentation of the results. We also wish to acknowledge very helpful discussions with D. R. Rummler and Drs. W. W. Kriegel, J. L. Whitfield, and R. A. Douglas.

LIST OF REFERENCES

1. Douglas, R. A., Bingham, W. L., Blake, H. W. and Liddell, W. L. (N. C. State University), "Experimental Method for Diffraction Studies During Impact," Technical Report 69-1, THEMIS Research Program on Materials Response Phenomena at High Deformation Rates, Contract N00014-68-A-0187, 41 pp., February, 1969.

2. Blake, H. W., Stadelmaier, H. H. and Douglas, R. A. (N. C. State University), "General Optical Diffraction-Strain," Technical Report 69-2, THEMIS Research Program on Materials Response Phenomena at High Deformation Rates, Contract N00014-68-A-0187, 46 pp., March, 1969.

3. Whitfield, J. K., Douglas, R. A. and Jeelani, S. (N. C. State University) "Powder Accelerator Systems for Axial Impact Studies," Technical Report 69-3, THEMIS Research Program on Materials Response Phenomena at High Deformation Rates, Contract N00014-68-A-0187, 23 pp., February, 1969.

4. Griffith, A. A., "Phenomena of rupture and flow in solids," Phil. Trans. Roy. Soc. (London) 221A 163-198 (1920).

5. Petch, N. J., Congleton, J., Hardie, H. and Perkins, R. N., "Effect of Surface Energy," Study of Brittle Behavior of Ceramic Materials, Technical Documentary Report No. ASD-TR-61-628, Part III, pp. 133-174 (1964).

6a. Clarke, F. J. P., Tattersall, H. G. and Tappin, G., "Toughness of ceramics and their work of fracture," Proc. Brit. Ceram. Soc. No. 6 163-172, June, 1966.

b. Tattersall, H. G. and Tappin, G., "Work of fracture and its measurement in metals, ceramics and other materials," J. Mater. Sci. 1 (3) 296-301 (1966).

7. Wiederhorn, S., (U. S. Bur. Standards), "The Double Cantilever Cleavage Technique," Presented U. S. Army Materials Research Agency Seminar on Structural Ceramics and Testing of Brittle Materials, IIT Research Institute, Chicago, Ill., March, 1967

8. Gutshall, P. L. and Gross, G. E., "Observations and mechanisms of fracture in polycrystalline alumina," Eng. Fract. Mech. [In Press].

9. Orowan, E., "Fracture and strength of solids," Repts. Prog. Phys. XII 185-232 (1948).

10. Cline, C. F. and Wilkins, M. F., "The Importance of Material Properties in Ceramic Armor," Paper presented in Symposium on Ceramic Armor Technology, Battelle Memorial Institute, Columbus, Ohio, January 29-30, 1969. [Confidential] To be published.

11. Marvin, D. M., "Penetration Mechanics," Paper presented in Symposium on Ceramic Armor Technology, Battelle Memorial Institute, January, 1969. [Confidential] To be published.

12. Taylor, J. W. and Hopson, J. W., "Plane Stress Waves in Some Refractory Compounds," Paper to be presented in Society Symposium 2 - Ceramic Armor, 71st Annual Meeting of the American Ceramic Society, Inc., Washington, D. C., May, 1969.

13. Spriggs, R. M., Vasilos, T. and Brissette, L. A., "Grain Size Effects in Polycrystalline Ceramics," Chapter 20 (pp. 313-344) in W. W. Kriegel and H. Palmour III, Eds., The Role of Grain Boundaries and Surfaces in Ceramics, Materials Science Research, Vol. 3 Plenum Press, New York, N. Y., 1966.

14. Mallinder, F. P. and Proctor, B. A., "Preparation of high-strength sapphire crystals," Proc. Brit. Ceram. Soc. No. 6 9-16, June, 1966.

15. Brenner, S. S., "Mechanical behavior of sapphire whiskers at elevated temperature," J. Appl. Phys. 33 (1) 33-39 (1962).

16. Kriegel, W. W., Palmour III, H. and Choi, D. M., "The Preparation and Mechanical Properties of Spinel," Chapter 12 (pp. 167-186) in Proceedings of a Symposium on Special Ceramics, 1964 (British Ceramic Research Association, Stroke-on-Trent, July, 1964), P. Popper, Ed., Academic Press (London) Ltd., 1965.

17. Lynch, J. F., Ruderer, C. G. and Duckworth, W. H. (Battelle Memorial Institute), Engineering Properties of Ceramics: Databook to Guide Materials Selection for Structural Applications. Technical Report AF ML-TR-66-52, June, 1966.

18. Proceedings of Conference on Ceramic Armor Technology. Sponsored by Air Force Materails Laboratory and Defense Ceramic Information Center, Battelle Memorial Institute, January, 1969. [Confidential] To be published.

19. Wachtman, J. B., Jr. and Maxwell, L. H., "Plastic deformation of ceramic oxide single crystals, I." J. Am. Ceram. Soc. 37 (7) 291-99 (1954); II., 40 (11) 377-85 (1957).

20a. Klassen-Neklyudova, M. V., "Plastic deformation of crystals of synthetic corundum," J. Tech. Phys. U.S.S.R. 12 519-51 (1942).

b. Klassen-Neklyudova, M. V., Ikornikova, N. and Tumilovskii, G. E., "Plastic Deformation of Synthetic Corundum Crystals," pp. 237-46 in Shubnikov, A. V., Klassen-Neklyudova, M. V. and Grum-Grhimailo, S. V. (Eds.). Physical Properties of Synthetic Corundum, A Symposium, 356 pp., Trudy Inst. Krist. Akad. Nauk. SSSR No. 8, 1953.

21. Scheuplein, R. J. and Gibbs, P., "Surface structure in corundum: I. Etching of dislocations," J. Am. Ceram. Soc. 43 (9) 458-72 (1960).

22a. Kronberg, M. L., "Polygonization of a plastically bent sapphire crystal," Sci. 122 (No. 3178) 599-600 (1955).

b. May, J. E., "Polygonization of Sapphire," Kinetics of High Temperature Processes (W. D. Kingery, Ed.), 30-37. The Technology Press of M.I.T. and John Wiley & Sons, Inc., New York, 1959.

23. Stephens, D. L. and Alford, W. J., "Dislocation structures in single crystal Al_2O_3," J. Am. Ceram. Soc. 47 (2) 55-60 (1964).

24. Janowski, J. R. and Conrad, H., "Dislocations in ruby laser crystals," Trans. A.I.M.E. 230 (4) 717-75 (1964).

25a. Davies, L. M., "Residual strain in sapphire rods and boules," Proc. Brit. Ceram. Soc. No. 6, 1-7, June, 1966.

b. Davies, C. M., "The effect of heat treatment on the tensile strength of sapphire," ibid. 29-35.

26. Day, R. B. and Stokes, R. J., "Grain Boundaries and the Mechanical Behavior of Magnesium Oxide," Chapt. 22 (pp. 355-386) in W. W. Kriegel and H. Palmour III, Eds., The Role of Grain Boundaries and Surfaces in Ceramics, Materials Science Research, Vol. 3, 631 pp., Plenum Press, New York, 1966.

27. Copley, S. M. and Pask, J. A., "Deformation of Polycrystalline Ceramics," Chapt. 13 (pp. 189-224), ibid.

28. Choi, D. M. and Palmour, H. III, "Fractographic Evidence of Multiple Slip in Deformed Hot Pressed Spinel," Chapt. 25 (pp 473-482), ibid.

29 Kronberg, M. L., "Dynamical flow properties of single crystals of sapphire I," J. Am. Ceram. Soc. 45 (6) 274-279 (1962).

30a. Stoefel, E. and Conrad, H., "Fracture and twinning in sapphire (Alpha-Al_2O_3 crystals)", Trans. A.I.M.E. 227 1053 (1963).

b. Conrad, H., Janowski, K. and Stoefel, E., "Additional observations on twinning in sapphire (alpha-Al_2O_3 crystals) during compression," Trans. A.I.M.E. 233 255 (1965).

c. Conrad, H., Stone, G. and Janowski, K., "Yielding and flow of sapphire (alpha Al_2O_3 crystals) in tension and compression," Trans. A.I.M.E. 233 889 (1965).

31. Heuer, A. H., "Deformation twinning in corundum," Phil. Mag. 13 (122) 379-393 (1966).

32. Bayer, P. D. and Cooper, R. E., "A new slip system in sapphire," J. Mater. Sci. 2 (3) 301 (1967).

33. Huckabee, M. L. and Palmour, H. III, "Kinking in Sapphire," Paper presented before the Summer Meeting of the Southeastern Section of the American Ceramic Society, Gatlinburg, Tenn., June, 1968 [Manuscript being prepared for publication].

34. Palmour, H. III, Kriegel, W. W., Becher, P. F., Chambers, H. B., Huckabee, M. L. and Huntley, W. S. (North Carolina State University), Grain Boundary Sliding in Alumina Bicrystals. Progress Report No. ORO-3328-9, Contract No. AT-(40-1)-3328, Division of Research, U. S. Atomic Energy Commission, 66 pp., December, 1968.

35. Bridgman, P. W., Large Plastic Flow and Fracture, 362 pp., McGraw-Hill Book Company, Inc., New York, 1952.

36. Palmour, H. III and Kriegel, W. W. (N. C. State University), Engineering Study Report, Brittleness in Ceramics, Part I: Dislocations in Single Crystal Sapphire as Revealed by Thermal Etching, 123 pp., June, 1961; Part II: The Influence of Diffused Transition Metal Oxides on the Micromechanical Properties of Single Crystal Sapphire, 133 pp. Contract DA-36-034-ORD-2645, June, 1961.

37. Palmour, H. III, Kriegel, W. W. and DuPlessis, J. J., "Micro-Brittleness Anisotropy in Thermally Etched Sapphire," pp. 313-327 in W. W. Kriegel and H. Palmour III, Eds., Mechanical Properties of Engineering Ceramics. Interscience Publishers, Inc., New York, 1961.

38. Palmour, H. III, DuPlessis, J. J. and Kriegel, W. W., "Microstructural features and dislocations on thermally etched sapphire surfaces." J. Am. Ceram. Soc. 44 (8) 400-404 (1961).

39. Hockey, B. J., "Observation of Plastic Deformation at Microhardness Indentations in Sapphire." Paper to be presented before Basic Science Division at the 71st Annual Meeting of the American Ceramic Society, Washington, D. C., May, 1969.

40. Palmour, H. III, "Properties and Applications of Ceramic Materials," pp. 793-832 in A. Standen, Exec. Ed., Kirk-Othmer Encyclopedia of Chemical Technology, Vol. 4, Second Edition, John Wiley and Sons, Inc., 1964.

41a. Meakin, J. D. and Petch, N. J., "Atomistic Aspects of Fracture," pp. 393-415 in D. C. Drucker and J. J. Gilman, Eds., Fracture of Solids, 708 pp., Interscience Publishers, Division of John Wiley & Sons, Inc., New York, 1963.

b. Westwood, A. R. C., "Effects of Environment on Fracture Behavior," pp. 553-603, ibid.

c. Parker, E. R., "Plastic Flow and Fracture of Crystalline Solids," pp 1-12 in Mechanical Behavior of Crystalline Solids, Nat'l. Bur. Standards Monograph 59, March, 1963.

42. Parikh, N. M., Ed. (IIT Research Institute, Chicago, Ill.), Studies of the Brittle Behavior of Ceramic Materials. Technical Documentary Report No. ASD-TR-61-628, Part III, 403 pp., June, 1964.

43 Carniglia, S. C., "Influences on Mechanical Behavior in Refractory Oxides," Chapter 24 (pp. 425-472) in W. W. Kriegel and H. Palmour III, Eds., The Role of Grain Boundaries and Surfaces in Ceramics, Materials Science Research, Vol. 3, Plenum Press, New York, 1966.

44. Spriggs, R. M., Mitchell, J. B. and Vasilos, T., "Mechanical properties of pure, dense aluminum oxide as a function of temperature and grain size," J. Am. Ceram. Soc. 47 (7) 323-327 (1964).

45. Petch, N. J., "The cleavage strength of polycrystals," J. Iron Steel Inst. 174 25 (1953).

46. Pears, D. C. (Southern Research Institute), "Strength Determinations of Brittle Materials," Paper presented at U. S. Army Materials Research Agency Seminar on Structural Ceramics and Testing of Brittle Materials, IIT Research Institute, Chicago, March, 1967.

47. Lewis, D. and Lindley, M. W., "Enhanced activity and the characterization of ball-milled alumina," J. Am. Ceram. Soc. 49 (1) 49-50 (1966).

48. Bergmann, D. R. and Barrington, J., "Effect of explosive shock waves on ceramic powders," J. Am. Ceram. Soc. 49 (9) 502-507 (1966).

49. Heckel, R. W. and Youngblood, J. L., "X-ray line broadening study of explosively shocked MgO and α-Al_2O_3 powders," J. Am. Ceram. Soc. 51 (7) 398-401 (1968).

50. Palmour, H. III, Bradley, R. A. and Johnson, D. R., "A Reconsideration of Stress and Other Factors in the Kinetics of Densification," Chapt. 22 (pp 392-407) in T. J. Gray and V. D. Frechette, Eds., Kinetics of Reaction in Ionic Systems, Materials Science Research, Vol. 4, Plenum Press, New York [In Press].

51a. Morgan, C. S. and Yust, C. S., "Materials transport during sintering of materials with the fluorite structure," J. Nucl. Mater. 10 182 (1963).

b. Morgan, C. S., McHargue, C. J. and Yust, S. C., "Materials transport in sintering," Proc. Brit. Ceram. Soc. No. 3, 177-84 (1965).

c. Morgan, C. S., "Comment on'Dorn method in the study of initial phase of uranium oxide sintering,'"J. Am. Ceram. Soc. 51 (12) 724 (1968).

52. Morgan, C. S., Densification Kinetics During Nonisothermal Sintering of Oxides, in T. J. Gray and V. D. Frechette, Eds., Kinetics of Reaction in Ionic Systems, Materials Science Research, Vol. 4, Plenum Press, New York [In Press].

53. Bruce, R. H. "Aspects of the Surface Energy of Ceramics I - Calculations of Surface Free Energies," Chapt. 24 (pp 359-367) in G. H. Stewart, Ed., Proceedings of the second Conference held under auspices of the British Ceramic Society and the Nederlandse Keramische Vereniging at Noordwijk aan Zee, May, 1963. 431 pp., Academic Press, 1965.

54. Congleton, J. and Petch, N. J., "Dislocation movement in the brittle fracture of alumina," Acta Metallurgica 14 (10) 1179-1182 (1966).

55. Wiederhorn, S. M. (Institute of Materials Research), Fracture of Sapphire, 46 pp., Contribution of the National Bureau of Standards, Washington, D. C., 1969.

56. McBrayer, R. D. and Palmour, H. III (N. C. State University), High Temperature Deformation of Alumina-Rich Spinel Single Crystals in Compression, 79 pp. Technical Report No. 3, Contract No. DA-31-124-ARO-D-207, U. S. Army Research Office-Durham, August, 1965.

57. Choi, D. M. and Palmour, H. III (N. C. State University), Flow and Fracture of Hot Pressed Polycrystalline Spinel at Elevated Temperatures, 88 pp. Technical Report No. 2, Contract No. DA-31-124-ARO-D-207, U. S. Army Research Office-Durham, August, 1965.

58. Palmour, H. III, "Multiple slip processes in magnesium aluminate at high temperature," Proc. Brit. Ceram. Soc. No. 6 209-224, June, 1966.

59. Palmour, H. III, Choi, D. M., Barnes, L. D., McBrayer, R. D. and Kriegel, W. W., "Deformation in Hot Pressed Polycrystalline Spinel," pp. 158-197 in H. H. Stadelmaier and W. W. Austin, Eds., The Proceedings of the Research Conference on Structure and Properties of Engineering Materials, Materials Science Research, Vol. 1, Plenum Press, New York, 1963.

60. Kriegel, W. W., Palmour, H. III and Choi, D. M., The Preparation and Mechanical Properties of Spinel, Chapt. 12 (pp 167-186) in P. Popper, Ed., Special Ceramics 1964, Academic Press (London) Ltd., 1965.

61. Chay, D. M., Palmour, H. III and Kriegel, W. W., "Microstructure and room temperature mechanical properties of hot pressed magnesium aluminate as described by quadratic multivariable analysis," J. Am. Ceram. Soc. 51 (1) 10-16 (1968).

62. Rummler, D. R. and Palmour, H. III, "Vacuum hot pressing of magnesium aluminate," J. Am. Ceram. Soc. 51 (6) 220-226 (1968).

63. Zapffe, C. A. and Clogg, M., Jr., "Fractography - a new tool for metallurgical research," Trans. Am. Soc. Metals 34 71 (1945).

64. Burghard, H. C., Jr. and Davidson, D. L., "Fracture Mechanisms and Fracture Surface Topography," pp. 571-596 in Yokobori, T., Kawasaki, T. and Swedlow, J. L., Eds., Vol. 2, Proceedings of the First International Conference on Fracture. The Japanese Society for Strength and Fracture of Materials. 1966.

65. Crussard, C., Plateau, J., Tamhanke R., Henry, G. and LaJeunesse, D., "A Comparison of Ductile and Fatigue Fracture," pp. 524-561 in Averbach, B. L., Felbeck, D. K., Hahn, G. T., and Thomas, D. A., Eds., Fracture, 646 pp., John Wiley & Sons, Inc., 1959.

66. Beachem, C. D., "An electron fractographic study of the influence of plastic strain conditions upon ductile rupture process in metals," Trans. Am. Soc. Metals 56 318-326 (1963).

67. Beachem, C. D. and Meyn, D. A., "Illustrated Glossary of Fractographic Terms, Section 2, Glide Plane Decohesion, Serpentine Glide, Ripples, Stretching, Microvoid Coalescence," NRL Memorandum Report 1547, U. S. Naval Research Laboratory, Washington, D. C., June, 1964.

68. Low, J. R., Jr., "A Review of the Microstructural Aspects of Cleavage Fracture," pp. 68-90 in Fracture, John Wiley & Sons, Inc., 1959.

69. Fisher, J. C., Johnston, W. G., Thompson, R. and Vreeland, T., Jr., Eds., Dislocations and Mechanical Properties of Crystals. 634 pp., John Wiley & Sons, Inc., New York, 1956.

70a. Kriegel, W. W. and Palmour, H. III, Eds., Mechanical Properties of Engineering Ceramics. 646 pp. Interscience Publishers, Inc., New York, London. 1961.

b. Newkirk, J. B. and Wernick, J. H., Eds. Direct Observation of Imperfections in Crystals. Interscience Publishers, a Division of John Wiley & Sons, Inc., New York, 1962.

71. Mechanical Behavior of Crystalline Solids. (Proceedings of an American Ceramic Society Symposium, New York, April, 1962) National Bureau of Standards Monograph 59, 113 pp. March, 1963.

72a. Stadelmaier, H. H. and Austin, W. W., Eds., The Proceedings of the Research Conference on Structure and Properties of Engineering Materials. Materials Science Research, Vol. 1, 335 pp. Plenum Press, New York, 1963.

b. Kriegel, W. W. and Palmour H. III, Eds., University Conferences on Ceramic Science - 1964: The Role of Grain Boundaries and Surfaces in Ceramics. Materials Science Research, Vol. 3, 631 pp. Plenum Press, New York, 1966.

73. Fulrath, R. M. and Pask, J. A., Ceramic Microstructures: Their Analysis, Significance and Production. 1008 pp., John Wiley & Sons, Inc., New York, 1968.

74. Kay, D. H., Ed. Techniques for Electron Microscopy. Second Edition, 560 pp. F. A. Davis Company, Philadelphia, Pa., 1965.

75. Thomas, G. Transmission Electron Microscopy of Metals. 299 pp. John Wiley & Sons, Inc., New York, 1962.

76. Amelinckx, S. The Direct Observation of Dislocations. 487 pp. Solid State Physics, Suppl. 6. Academic Press, New York, London, 1964.

77. Heidenreich, R. D. Fundamentals of Transmission Electron Microscopy. Interscience Monographs and Texts in Physics and Astronomy, Vol. XIII. 414 pp. John Wiley & Sons, Inc., New York, 1964.

78. Hirsch, P. B., Howie, A., Nicholson, R. B., Pashley, D. W. and Whelan, M. J. Electron Microscopy of Thin Crystals. 549 pp. Plenum Press, New York, 1965.

79. Voruz, T. A., Jewett, R. P. and Accountius, O. E., "Direct observations of dislocations in sapphire," J. Am. Ceram. Soc. 46 (9) 459-460 (1963).

80. Barber, D. J., "Electron microscopy and diffraction of aluminum oxide whiskers," Phil. Mag. 10 75-94 (1964).

81. Mehan, R. L. and Feingold, E., "Strength and Structure of Very Fine Sapphire Whiskers," Chapt. 15 (pp. 355-406) in J. J. Burke, N. L. Reed, and V. Weiss, Eds., Strengthening Mechanisms: Metals and Ceramics. Proceedings of the 12th Sagamore Army Materials Research Conference, Syracuse University Press, 1966.

82. Tighe, W. J., "Jet thinning device for preparation of Al_2O_3 electron microscope specimens," Rev. Sci. Inst. 35 520-21 (1964).

83. Barber, D. J. and Tighe, N. J., "Observations of dislocations and surface features in corundum crystals by electron transmission microscopy," J. Research Nat. Bur. Standards 69A (3) 271-280 (1965).

84. Barber, D. J. and Tighe, N. J., "Electron microscopy and diffraction of synthetic corundum crystals: I. Pure aluminum oxide grown by the Verneuil process." Phil. Mag. 11 495-512 (1965).

85. Barber, D. J. and Tighe, N. J., "Electron Microscopy and diffraction of synthetic corundum crystals: II. Dislocations and grain boundaries in impurity doped aluminum oxide." Phil. Mag. 14 (129) 531-544 (1966).

86a. Wilks, R. S., Desport, J. A. and Bradley, R. (Ceramics Group, Atomic Energy Research Establishment, Harwell), Transmission Electron Microscopy of Neutron Irradiated Alpha-Al_2O_3 Single Crystals. Research Group Report AERE-R 5103, 26 pp., United Kingdom Atomic Energy Authority, 1965.

86b. Wilks, R. S. (Ceramics Division, Atomic Energy Research Establishment, Harwell), Neutron-Induced Damage in α-Al_2O_3, BeO, and MgO. Research Group Report AERE-R5543, 154 pp., United Kingdom Atomic Energy Authority, 1967.

87. Paulus, M. and Reverchon, F., J. Phys. Radium 22 (Suppl. 6) 103A-107A (1961).

88. Paulus, M., Supplemental Note to Chapter 12 [by M. C. Inman], pp. 183-186 in W. W. Kriegel and H. Palmour III, Eds., The Role of Grain Boundaries and Surfaces in Ceramics, Materials Science Research, Vol. 3, Plenum Press, New York, 1966.

89. Tighe, N. J. and Hyman, A., "Transmission Electron Microscopy of Alumina Ceramics," pp. 121-136 in Anisotropy in Single Crystal Refractory Compounds, Vol. 2., F. W. Vahldiek and S. A. Mersal, Eds. Plenum Press, New York, 1968.

90. Tighe, N. J., "Observations in polycrystalline ceramics by electron transmission microscopy," pp. 420-21 in Proceedings of the 26th Annual Meeting of the Electron Microscopy Society of American, September, 1968.

91a. Tighe, N. J. and Heuer, A. H., "Substructure of hot-pressed polycrystalline Al_2O_3," Paper presented before Basic Science Division, 70th Annual Meeting of the American Ceramic Society, Chicago, April, 1968.

b. Tighe, N. J. and Kreglo, J. R., Jr., "Microstructure of MgO Brick," Paper presented at the 70th Annual Meeting of the American Ceramic Society, Chicago, April, 1968.

92. Smothers, W. J. and Chaing, Y., Handbook of Differential Thermal Analysis. 633 pp. Chemical Publishing Co., Inc., New York, 1966.

93. David, D. J., "Introduction to theory and application of DTA and considerations of Stone instrumentation features," Laboratory Equipment Digest, April, June, 1968.

94. Campbell, W. B., "Dynamic Thermal Analysis," in Kinetics of Reaction in Ionic Systems (T. J. Gray and V. D, Frechette, Eds.) Materials Sciences Research, Vol. 4, Plenum Press, New York (In Press).

95. Brammar, L. S. and Dewey, M. A. P., Specimen Preparation for Electron Metallography. 110 pp. American Elsevier Publishing Company, Inc., New York, 1966.

96. Witter, D. E. and Palmour, H. III, "Tabulation of Indices and Interplanar Angles for Rapid Identification of Crystallographic Planes," pp 67-101 in Anisotropy on Single Crystal Refractory Compounds, Vol. 1, F. W. Vahldick and S. A. Mersol, Eds., Plenum Press, New York, 1968.

97. Witter, D. E. and Palmour, H. III, PIMAX Tables for Alpha Alumina. Engineering School Bulletin No. 84, North Carolina State University at Raleigh, 1967.

98. Lewis, M. H., "Microstructure of magnesium oxide cleavage surfaces," Phil. Mag. 13 [126] 1123-30 (1966).

99. Gutshall, P. L., Gross, G. E. and Swanson, G. D. (Midwest Research Inst.), A Study of the Physical Basis of Mechanical Properties of Ceramics. Air Force Materials Laboratory Technical Report AFML-TR-67-99, Contract AF 33(615)-2669, June, 1967.

100. Gutshall, P. L. and Shaw, G. G., "Alumina Fractured Surfaces as Revealed by Direct Replication Technique," pp. 282-283 in Proceedings of the 25th Annual Meeting of the Electron Microscope Society of America. September, 1967.

101a. Kingery, W. D., "Densification during sintering in the presence of a liquid phase: I. Theory," J. Appl. Phys. 30 (3) 301-306 (1959).

b. Kingery, W. D. and Narasimhan, M. D., "Densification during sintering in the presence of a liquid phase: II. Experimental," J. Appl. Phys. 30 (3) 307-310 (1959).

c. Kingery, W. D., Chapter 12 (particularly pp. 386-389) in Introduction to Ceramics. John Wiley and Sons, Inc., New York. 1960

d. Kingery, W. D., "Sintering in the Presence of a Liquid Phase," Chapter 24 (pp. 187-194) in W. D. Kingery, Ed., Kinetics of High Temperature Processes. 326 pp. The Technology Press of M.I.T. and John Wiley & Sons, Inc., New York, 1959.

e. Kingery, W. D., "Sintering in the Presence of a Liquid Phase," Chapter 16 (pp. 131-143) in W. D. Kingery, Ed., Ceramic Fabrication Processes. 235 pp. The Technology Press of M.I.T. and John W. Wiley & Sons, Inc., New York, 1960.

102. Coble, R. L., "Effect of Microstructure on the Mechanical Properties of Ceramic Materails," Chapt. 22 (pp 213-228) in W. D. Kingery, Ed., Ceramic FabricationProcesses. 235 pp. The Technology Press of M.I.T. and John Wiley & Sons, Inc., New York, 1960.

103. Binns, D. B. and Popper, P., "Mechanical properties of some commercial alumina ceramics," Proc. Brit. Ceram. Soc. No. 6 71-82, June, 1966.

104a. Poncelet, E. F., "Fracture and comminution of brittle solids," Trans. A.I.M.E. 169 (1946).

b. Poncelet, E. F., The Mechanism of Fracture Propagation, Technical Report, 25 pp., Poulter Laboratories of Stanford Research Inst., Menlo Park, Calif., July 1963.

105. Ohlberg, S. M., Bolob, H. R. and Hollabaugh, C. M., "Fractography of glasses evidencing liquid-in-liquid colloidal immiscibility." J. Am. Ceram. Soc. 45 (1) 1-4 (1962).

106. Amelinckx, S. and DeLavignette, P., "Electron Microscopic Observation of Dislocations in Silicate Layer Structures," Chapter 9 (pp. 105-123) in W. W. Kriegel and H. Palmour III, Eds., Mechanical Properties of Engineering Ceramics. 646 pp. Interscience Publishers, Inc., New York, London, 1961.

107. Congleton, J., Holdsworth, M. C. and Petch, N. J. (University of Newcastle-upon-Tyne), The Brittle Fracture of Alumina. 56 pp. Final Technical Report, Contract No. DAJA-37-67-C-0522, European Research Office, U. S. Army. April, 1968.

108a. Hornstra, J., "Dislocations Stacking Faults and Twins in the Spinel Structure," J. Phys. Chem. Solids 15 311-323 (1960).

b. Hornstra, J., "Dislocations in Spinels and Related Structures," pp. 88-97 in H. H. Stadelmaier and W. W. Austin, Eds. The Proceedings of the Research Conference on Structure and Properties of Engineering Materials, Materials Science Research, Vol. 1., 335 pp., Plenum Press, New York, 1963.

109. Kronberg, M. L., "Plastic deformation of single crystals of sapphire: basal slip and twinning." Acta Met. 5 (9) 507-24, 1957.

110. Swanson, G. D. and Gross, G. E. (Midwest Research Inst.), Physical Parameters Affecting Fracture Strength and Fracture Mechanisms in Ceramics. Final Report, Contract No. N00019-68-C-0127, U. S. Navy, Naval Air Systems Command. 37 pp., November, 1968.

111. Guard, R. W. and Romo, P. C., "X-Ray Microbeam Studies of Fracture Surfaces in Alumina," J. Am. Ceram. Soc. 48 (7) (1965)

112. Parker, E. A., "Future Prospects for Structural Ceramics," Chapt. 1 (pp. 1-6) in W. W. Kriegel and H. Palmour III, Eds., Mechanical Publishers, Inc., New York, London, 1961.

General References on Electron Fractography

113. Beachem, C. D. and Pelloux, R. M. N., Electron Fractography - A tool for the study of micromechanism of fracturing processes (pp. 210-245), in ASTM Special Technical Publication No. 381, Fracture Toughness Testing and Its Applications. 409 pp. American Society for Testing and Materials, Philadelphia, 1965.

114. Phillips, A., Kerlins, V. and Whiteson, B. V., Electron Fractography Handbook. Technical Report ML-TDR-64-416, 897 pp. Air Force Materials Laboratory Research and Technology Division Air Force System Command Wright-Patterson Air Force Base, Ohio, 1965.

115. Pelloux, R. M. N. and McMillan, J. C., "The analysis of fracture surfaces by electron microscopy," (pp. 548-569) in T. Yokobori, T. Kawasaki and J. L. Swedlow, Eds., Proceedings of the First International Conference on Fracture, Vol. 2 (pp. 501-1109). The Japanese Society for Strength and Fracture of Materials, Japan, 1966.

116. Bucher, J. H., "A micro-fractographic analysis of fracture surfaces in some ultra-high-strength steels," Paper 9 (pp. 323-371) in H. D. Greenberg, Ed. Application of Fracture Toughness Parameters to Structural Metals. Metallurgical Society Conferences. Vol. 31, 406 pp. Gordon and Breach Science Publishers, New York, 1966.

Unclassified
Security Classification

DOCUMENT CONTROL DATA - R&D

(Security classification of title, body of abstract and indexing annotation must be entered when the overall report is classified)

1. ORIGINATING ACTIVITY (Corporate author) NORTH CAROLINA STATE UNIVERSITY Raleigh, North Caroline	2a. REPORT SECURITY CLASSIFICATION Unclassified 2b. GROUP

3. REPORT TITLE

Fractographic and Thermal Analyses of Shocked Alumina

4. DESCRIPTIVE NOTES (Type of report and inclusive dates)

5. AUTHOR(S) (Last name, first name, initial)

H. Palmour III, C. H. Kim, D. R. Johnson, C. E. Zimmer

6. REPORT DATE	7a. TOTAL NO. OF PAGES	7b. NO. OF REFS
April 1969	104	116

8a. CONTRACT OR GRANT NO.	9a. ORIGINATOR'S REPORT NUMBER(S)
N00014-68-A-0187 b. PROJECT NO.	69-5
c. d.	9b. OTHER REPORT NO(S) (Any other numbers that may be assigned this report)

10. AVAILABILITY/LIMITATION NOTICES

Qualified requesters may obtain copies of this report from DDC.

11. SUPPLEMENTARY NOTES	12. SPONSORING MILITARY ACTIVITY
	Advanced Research Projects Agency Washington, D. C.

13. ABSTRACT

This report is concerned with energy absorption processes in ceramic materials exposed to highly dynamic strains capable of causing fracture. Optical and electron fractographic analyses, and direct transmission electron microscopy, were employed in characterizing fracture in ballistically damaged sapphire single crystals and alumina ceramics. Impact fractures were compared with slow break fractures in bars cut from large polycrystalline fragments. Using electron microscopic and dynamic differential calorimetry techniques, explosively shocked alumina particulates also have been examined for evidences of residual strain and annealable excess energy.

The findings produced many mutually supporting evidences of local plastic deformation and energy absorption associated with fracture processes in aluminum oxide ceramics and sapphire single crystals. It was concluded that truly brittle cracks--those which can be propagated with fracture surface energy (γ_f) comparable to the calculated surface free energy (γ_s) without doing work upon the bulk of the material traversed--are relatively rare in this refractory oxide. Rather, fractures commonly observed in α-Al_2O_3 were propagated (at least in part) as almost ductile or blunted cracks--those in which the fracture surface energy (γ_f) has been substantially increased above the nominal surface free energy (γ_s) because of plastic work energy (γ_p) which has to be expended in deforming bulk material at and near the advancing crack front. Microscopic evidences from replication fractography, and particularly from direct transmission electron microscopy, strongly

DD FORM 1 JAN 64 1473

Unclassified
Security Classification

Unclassified
Security Classification

14 KEY WORDS	LINK A		LINK B		LINK C	
	ROLE	WT	ROLE	WT	ROLE	WT
Ceramic Armor						
Alumina Crystals and Ceramics						
Spinel ($MgAl_2O_4$) Ceramics						
Impact Energy and Ballistic Damage						
Explosive Shock						
Brittleness and Fractography						
Optical and Transmission Electron Microscopy						
Replication Techniques						
Brittle Fracture Modes						
Fracture-induced Plastic Deformation						
Dislocations in Shocked Alumina						
Surface Free Energy						
Plastic Work Energy						
Fracture Surface Energy						
Residual Strain Energy						
Dynamic Differential Calorimetry						

INSTRUCTIONS

1. ORIGINATING ACTIVITY: Enter the name and address of the contractor, subcontractor, grantee, Department of Defense activity or other organization *(corporate author)* issuing the report.

2a. REPORT SECURITY CLASSIFICATION: Enter the overall security classification of the report. Indicate whether "Restricted Data" is included. Marking is to be in accordance with appropriate security regulations.

2b. GROUP: Automatic downgrading is specified in DoD Directive 5200.10 and Armed Forces Industrial Manual. Enter the group number. Also, when applicable, show that optional markings have been used for Group 3 and Group 4 as authorized.

3. REPORT TITLE: Enter the complete report title in all capital letters. Titles in all cases should be unclassified. If a meaningful title cannot be selected without classification, show title classification in all capitals in parenthesis immediately following the title.

4. DESCRIPTIVE NOTES: If appropriate, enter the type of report, e.g., interim, progress, summary, annual, or final. Give the inclusive dates when a specific reporting period is covered.

5. AUTHOR(S): Enter the name(s) of author(s) as shown on or in the report. Enter last name, first name, middle initial. If military, show rank and branch of service. The name of the principal author is an absolute minimum requirement.

6. REPORT DATE: Enter the date of the report as day, month, year; or month, year. If more than one date appears on the report, use date of publication.

7a. TOTAL NUMBER OF PAGES: The total page count should follow normal pagination procedures, i.e., enter the number of pages containing information.

7b. NUMBER OF REFERENCES: Enter the total number of references cited in the report.

8a. CONTRACT OR GRANT NUMBER: If appropriate, enter the applicable number of the contract or grant under which the report was written.

8b, 8c, & 8d. PROJECT NUMBER: Enter the appropriate military department identification, such as project number, subproject number, system numbers, task number, etc.

9a. ORIGINATOR'S REPORT NUMBER(S): Enter the official report number by which the document will be identified and controlled by the originating activity. This number must be unique to this report.

9b. OTHER REPORT NUMBER(S): If the report has been assigned any other report numbers *(either by the originator or by the sponsor)*, also enter this number(s).

10. AVAILABILITY/LIMITATION NOTICES: Enter any limitations on further dissemination of the report, other than those imposed by security classification, using standard statements such as:

(1) "Qualified requesters may obtain copies of this report from DDC."

(2) "Foreign announcement and dissemination of this report by DDC is not authorized."

(3) "U. S. Government agencies may obtain copies of this report directly from DDC. Other qualified DDC users shall request through _____."

(4) "U. S. military agencies may obtain copies of this report directly from DDC. Other qualified users shall request through _____."

(5) "All distribution of this report is controlled. Qualified DDC users shall request through _____."

If the report has been furnished to the Office of Technical Services, Department of Commerce, for sale to the public, indicate this fact and enter the price, if known.

11. SUPPLEMENTARY NOTES: Use for additional explanatory notes.

12. SPONSORING MILITARY ACTIVITY: Enter the name of the departmental project office or laboratory sponsoring *(paying for)* the research and development. Include address.

13. ABSTRACT: Enter an abstract giving a brief and factual summary of the document indicative of the report, even though it may also appear elsewhere in the body of the technical report. If additional space is required, a continuation sheet shall be attached.

It is highly desirable that the abstract of classified reports be unclassified. Each paragraph of the abstract shall end with an indication of the military security classification of the information in the paragraph, represented as *(TS), (S), (C), or (U)*.

There is no limitation on the length of the abstract. However, the suggested length is from 150 to 225 words.

14. KEY WORDS: Key words are technically meaningful terms or short phrases that characterize a report and may be used as index entries for cataloging the report. Key words must be selected so that no security classification is required. Identifiers, such as equipment model designation, trade name, military project code name, geographic location, may be used as key words but will be followed by an indication of technical context. The assignment of links, roles, and weights is optional.

Unclassified
Security Classification